nature communications

Article

https://doi.org/10.1038/s41467-025-62565-5

SERBP1-PCIF1 complex-controlled m6Am modification in glutamatergic neurons of the primary somatosensory cortex is required for neuropathic pain in mice

Received: 4 October 2024

Accepted: 24 July 2025

Published online: 05 August 2025

Check for updates

Yue Huang[1,2,3,7], Gan Ma[1,2,3,7], Shan Xie[1,2,3,7], Runa Wei[1], Ya Liu[1], Ying Zeng[1], Yaxuan Zhao[1], Qihui Wang[1], Li Yang[1], Huiying Huang[1], Lingyun Hao[1], Xiaotian Zhao[1], Hongjun Wang[1], Wen Shen[1,4], Stanley Sau Ching Wong[5], Jun-Li Cao[1,2,3,8] ✉, Yuan-Xiang Tao[6,8] ✉ & Zhi-Qiang Pan[1,2,3,8] ✉

Nerve injury-induced changes in pain-associated genes contribute to genesis of neuropathic pain and comorbid anxiety. Phosphorylated CTD interacting factor-1 (PCIF1)-triggered N6, 2′-O-dimethyladenosine (m^6Am) mRNA modification represents an additional layer of gene regulation. However, the role of PCIF1 in these disorders is elusive. Here, we report PCIF1 is increased in glutamatergic neurons of the hindlimb region of the primary somatosensory cortex in mouse with neuropathic pain and anxiety, but not inflammatory pain or anxiety alone. Serpine-1 mRNA-binding protein-1 (SERBP1) is identified as a PCIF1 cofactor, their complex mediates m^6Am deposition onto mRNA. Blocking SERBP1-PCIF1 upregulation in glutamatergic neurons of the hindlimb region of the primary somatosensory cortex abolishes m^6Am gain on maf1 homolog, negative regulator of RNA polymerase III *(Maf1)*, elevates MAF1 protein, and mitigates neuropathic pain and anxiety. Conversely, mimicking this increase adds m^6Am onto *Maf1*, reduces MAF1, and induces comorbidity symptoms. These findings highlight the significance of m^6Am in neuropathic pain-anxiety comorbidity and identify SERBP1–PCIF1 in glutamatergic neurons of the hindlimb region of the primary somatosensory cortex as a potential therapeutic target.

Nerve injury-induced neuropathic pain, a chronic and refractory disease, affects 7–10% of the world's population[1,2]. What is worse is that approximately one-third of neuropathic pain patients have clinically relevant emotional symptoms such as anxiety. The latter further increases the difficulty of treating neuropathic pain and leads to a further decline in the patients' quality of life[3]. Current treatments for neuropathic pain have the limited effectiveness and/or produce severe adverse effects, partially due to unclear and complex mechanisms underlying the comorbidity of pain and anxiety. Among many brain regions associated with nociceptive sensation and emotion processing[4], primary somatosensory cortex (S1) is known to be crucial for pain and emotional modulation[5]. Clinical and preclinical studies have shown abnormal activation of S1 neurons in chronic neuropathic pain patients[6–8] and in animal models of neuropathic pain[9,10]. Comorbid neuropathic pain and anxiety are triggered at least in part through abnormal hyperexcitability and ectopic discharges in S1 neurons[11]. Recently developed strategies have enabled the precise pinpointing of neuronal function in individual layers of S1 in the sensation and

A full list of affiliations appears at the end of the paper. ✉e-mail: caojl0310@aliyun.com; yuanxiang.tao@njms.rutgers.edu; zhiqiangp2002@aliyun.com

emotional progression of nociception[12,13]. Therefore, understanding the dysregulation of genes in specific S1 neurons may provide targeted approaches for the management of neuropathic pain and anxiety disorders.

mRNA modification plays an important role in the regulation of gene expression[14]. N6-methyl-2′-O-methyladenosine (m^6Am) is one of the most prevalent mRNA modifications[14–16]. The m^6Am site is located at the first transcribed nucleotide adjacent to the m^7G cap in the 5′-UTR of mRNA[17,18]. Like m^6A methylation, m^6Am RNA modification represents an additional layer of reversible and dynamic gene regulation. Phosphorylated CTD interacting factor 1 (PCIF1) was recently identified as the sole known specific N6-methyltransferase for m^6Am. RNA m^6Am is written by PCIF1 and erased by fat-mass and obesity-associated protein (FTO) and is involved in mRNA stability, transcription, and translation[19–22]. PCIF1 interacts with C-terminal binding protein 2 (CTBP2) to facilitate m^6Am deposition in mRNA[23], suggesting the potentially important role of CTBP2 in PCIF1 control of m^6Am. Therefore, PCIF1- or FTO-induced dysregulation of m^6Am modification may produce physiological defects and participate in the pathological processes underlying various diseases[24–28]. However, it remains unknown whether and how m^6Am has a critical role in neuropathic pain. Serpine1 mRNA-binding protein 1 (SERBP1) is recently discovered to have chaperone-like properties, and plays crucial role in mRNA stability[29]. Increasing evidence have linked SERBP1 to brain function and development, especially neurogenesis and synaptogenesis[30–32]. Yet, it is elusive whether SERBP1 is involved in neuropathic pain.

Here we demonstrate that peripheral nerve injury induces a selective upregulation of PCIF1 protein (but not FTO) within glutamatergic neurons of the hindlimb region of primary somatosensory cortex ($S1HL^{Glu}$). This PCIF1 elevation is both necessary and sufficient for the induction and maintenance of neuropathic pain hypersensitivity. Crucially, we establish SERBP1 as an essential cofactor that collaborates with PCIF1 to mediate m^6Am deposition on target mRNAs in $S1HL^{Glu}$ neurons under neuropathic pain-anxiety comorbidity conditions. The SERBP1-PCIF1 complex exerts its effects, at least partially, through adding m^6Am modifications on maf1 homolog, negative regulator of RNA polymerase III (*Maf1*) mRNA. This epigenetic alteration leads to decreased MAF1 expression in $S1HL^{Glu}$ neurons. These findings suggest that the SERBP1-PCIF1 complex may serve as a promising therapeutic target for addressing the comorbidity of neuropathic pain and anxiety disorders.

Results

Peripheral nerve injury results in the increases in m^6Am and PCIF1 in primary somatosensory cortex

To mimic clinical neuropathic pain in the patients, we conducted the spared nerve injury (SNI) model in mice. Consistent with previous studies[33], after SNI surgery, mechanical allodynia as shown by an increase in paw withdrawal frequency (PWF) to 0.07 g and 0.4 g von Frey stimuli and heat hyperalgesia (Supplementary Fig. 1a–d). In addition, its comorbid anxiety-like behaviors occurred on day 21 after SNI demonstrated by spending less time in the central area in the open field (OFT) test (Supplementary Fig. 1e, f) and in the open arms with having fewer open-arm entries in the elevated plus maze (EPM) test (Supplementary Fig. 1h–j). As expected, locomotor function is intact in all SNI and sham mice (Supplementary Fig. 1g). These observations indicate that SNI successfully results in neuropathic pain and anxiety-like behaviors.

To determine the dynamics of mRNA modifications in the primary somatosensory cortex of the hind limb (S1HL) after peripheral nerve injury, we first examined the levels of m^6A, m^6Am, ac^4C, m^5C, and m^7G in S1HL mRNA on day 7 (initial phase) and day 21 (maintenance phase) after SNI surgery. The LC–MS/MS assay showed that the levels of m^6Am and m^7G were significantly increased in S1HL on days 7 and 21 post-SNI, the level of m^6A was also markedly decreased on day 21 after SNI (Fig. 1a). These observations suggest that m^6Am and m^6A in S1HL may be implicated in the genesis of neuropathic pain. To further examine how m^6Am and m^6A are changed in S1HL after SNI, we analyzed the expression of three RNA methyltransferases (PCIF1 for m^6Am; METTL3 and METTL14 for m^6A) and 2 RNA demethylases (FTO for m^6Am; ALKBH5 and FTO for m^6A) in the S1HL after surgery and found that only the level of PCIF1 was markedly increased in contralateral S1HL on day 7 or day 21 after SNI (Fig. 1b). This increase was also observed on days 3, 14, 28 and 35 after SNI (Fig. 1c), as well as was seen on day 14 in S1HL of SNI female mice (Supplementary Fig. 1k). However, levels of neither m^6Am nor PCIF1 protein were altered in the ipsilateral S1HL (Supplementary Fig. 1l, m) or in the contralateral primary motor cortex (M1), which is adjacent to the S1HL (Supplementary Fig. 1n, o), post-SNI. Consistently, the amount of *Pcif1* mRNA in the contralateral S1HL was increased from day 7 to 35 after SNI (Fig. 1d). Similar results were observed in another preclinical mouse model of chronic constriction injury (CCI)-induced neuropathic pain (Fig. 1e, f), as well as in the cisplatin injection-induced chemotherapy neuropathic pain model (Fig. 1g) and in the type 2 diabetes mellitus model caused by high-fat diet-induced obesity (Fig. 1h). Interestingly, the level of PCIF1 was not substantially changed in the contralateral S1HL in animal model of chronic inflammatory pain caused by plantar injection of complete Freund's adjuvant (CFA) from 2 hour to day 7 post-CFA (Fig. 1i). No change in PCIF1 level in contralateral S1HL was also observed from 10 min to 24 h after formalin injection (Fig. 1j). In addition, the expression of S1HL PCIF1 was not significantly altered after the mice were subjected to 10 days of chronic restraint stress (CRS) (Fig. 1k), a well-established rodent model of anxiety[34]. Additionally, due to the concurrent elevation of both m^7G and m^6Am levels, we examined the expression of the m^7G methyltransferase METTL1. The Western blot results revealed a significant increase in METTL1 expression in the contralateral S1HL following SNI (Supplementary Fig. 1p). Taken together, these data suggest that PCIF1 upregulation in S1HL is neuropathic pain-specific and that this upregulation may be responsible for m^6Am increase in S1HL under neuropathic pain conditions.

Increased PCIF1 in S1 is restricted to layer 5 excitatory neurons

Next, we examined the distribution pattern of the upregulated PCIF1 in S1HL. Double immunofluorescent labeling assays showed that approximately 81.3% of PCIF1-labelled-cells were positive for NeuN (a marker specific to neurons) and 8.6% for S100β (a marker of astrocytes) (Fig. 1l, m). None of PCIF1-labelled cells were positive for Iba1 (a marker of microglia). It is evident that PCIF1 is expressed predominantly in neurons in S1HL. The neurons in layers 2/3, 5, and 6 of S1HL have different functions and different responses to nociceptive signals[13,35–37]. To determine which layers and neuronal types[38] are involved in PCIF1 expression in neuropathic pain, we cross-bred the $tdTomato^{fl/fl}$ mice with *CaMK2α-Cre* mice or *Vgat-Cre* mice to label excitatory and inhibitory neurons, respectively, in the different layers of S1HL[39,40] and then individually collected these neurons from specific layers for single-cell RT-PCR assay of *Pcif1* mRNA 21 days after SNI or sham surgery (Fig. 1n; Supplementary Fig. 1q, r). Contralateral excitatory (glutamatergic) neurons from layer 5 of S1HL ($S1L5^{Glu}$) exhibited a marked increase in the level of *Pcif1* mRNA on day 21 after SNI surgery, whereases $S1L2/3^{Glu}$ and $S1L6^{Glu}$ neurons showed no change in *Pcif1* mRNA expression after SNI surgery (Fig. 1o). The amount of *Pcif1* mRNA was not altered in inhibitory neurons in layers 2/3, 5, or 6 (Fig. 1p). To further validate these findings, we employed laser capture microdissection[41] and selectively isolated fluorescence-labeled excitatory and inhibitory neurons from layers 2/3, 5, and 6. Consistent with the observations from single-cell RT-PCR assay, *Pcif1* mRNA was significantly increased only in $S1L5^{Glu}$ neurons (Supplementary Fig. 1t, u). These results indicate that SNI-induced increase of *Pcif1* mRNA occurs specifically in the glutamatergic neurons of S1HL layer 5.

https://doi.org/10.1038/s41467-025-62565-5

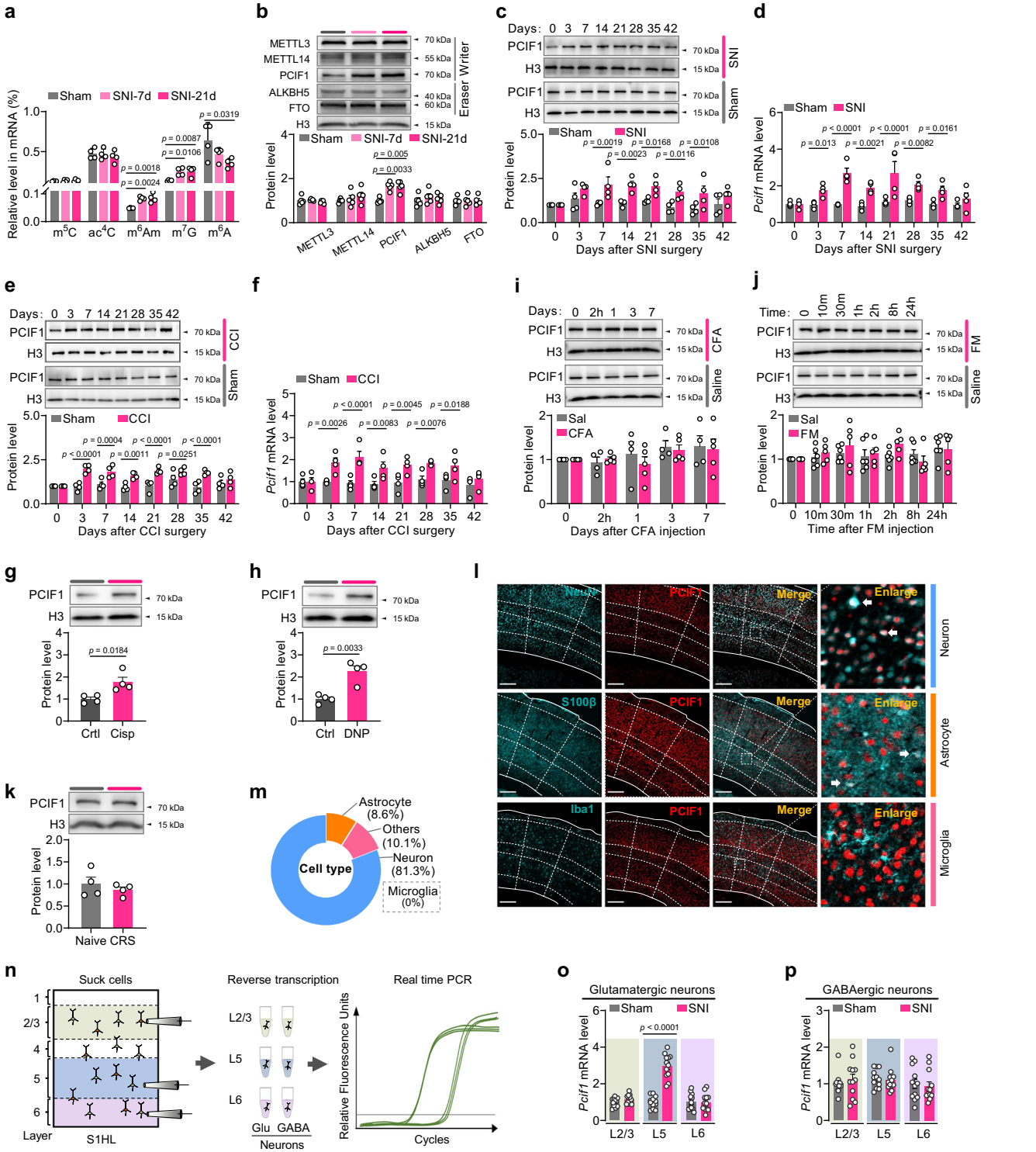

Fig. 1 | Neuropathic pain increases the levels of m^{6}Am and PCIF1 protein in S1HL. a m^{5}C, ac^{4}C, m^{6}Am, m^{7}G, and m^{6}A levels in contralateral primary somatosensory cortex (S1HL) on days 7 and 21 after surgery (n = 8 mice). **b** Expression level of METTL3, METTL14, PCIF1, ALKBH5, and FTO protein in the contralateral S1HL after surgery (n = 10 mice). **c**, **e** Expression of PCIF1 protein in contralateral S1HL at different times after spared nerve injury (SNI; n = 10 mice) or chronic constriction injury (CCI; n = 8 mice) or sham surgery. **d**, **f** Quantitative analysis of *Pcif1* mRNA expression in contralateral S1HL by qRT-PCR at different times post-SNI or post-CCI or sham surgery (n = 8 mice). **g**–**k** Expression of PCIF1 protein in contralateral S1HL in a model of cisplatin-induced neuropathic pain (Cisp), diabetic neuropathic pain (DNP) or chronic restraint stress (CRS) (n = 8 mice). **i**, **j** Expression of PCIF1 protein in contralateral S1HL at different times after complete Freund's adjuvant (CFA)injection (Saline group: n = 8 mice, CFA group: n = 10 mice) or formalin (FM) injection (Saline group: n = 12 mice, FM group: n = 10 mice). **l**, **m** Co-expression analysis of PCIF1 with neuron (NeuN), astrocyte (S100β) or microglia (Iba1) immunofluorescence staining in S1HL of naïve mice (n = 4 mice). Scale bar, 200 μm. **n** Schematic showing isolation of GABAergic neurons and glutamatergic neurons from the L2/3, L5, and L6 layers of S1HL of mice subjected to SNI surgery for quantitative analysis of *Pcif1* mRNA expression. **o**, **p** Expression of *Pcif1* mRNA in GABAergic or glutamatergic neurons of S1 layers 2-6. n = 12 single cells form mice. The data are represented as mean ± SEM. For RNA modifications, mRNA and protein, S1 samples from two mice were pooled to create one sample. One-way ANOVA followed with Dunnett's post hoc test was used for panels (**a**, **b**). Two-way ANOVA followed with Fisher's LSD post hoc test was used for panels (**c**–**f**, **i**, **j**, **o** and **p**). Student's unpaired t-test (two-tailed) was used for panels (**g**, **h** and **k**).

https://doi.org/10.1038/s41467-025-62565-5

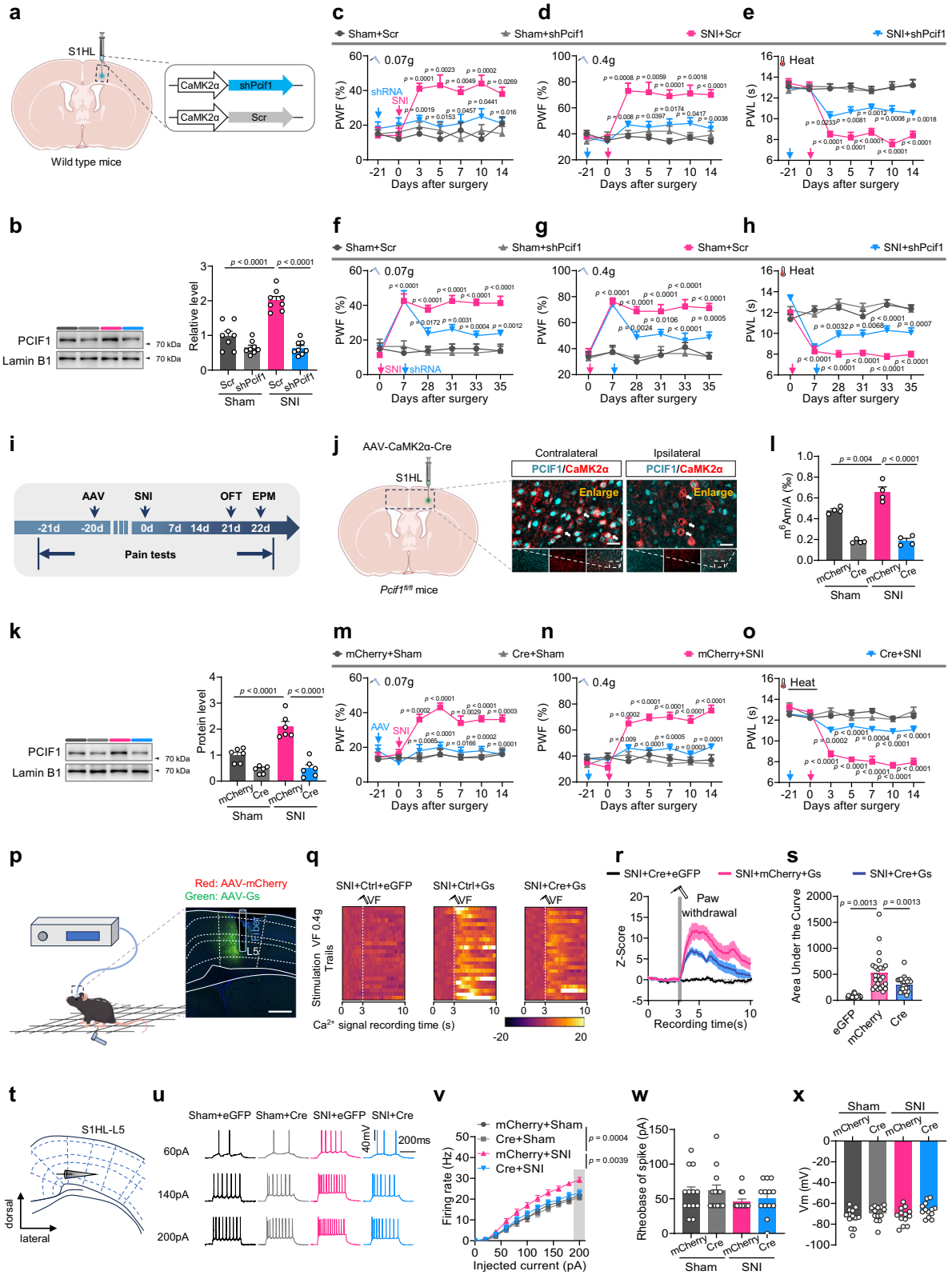

Blocking PCIF1 upregulation in S1HL^{Glu} neurons attenuates the SNI-induced nociceptive hypersensitivity

Does the upregulated PCIF1 in S1HL^{Glu} neurons participate in nerve injury-induced nociceptive hypersensitivity? To this end, we examined the effect of specifically blocking the PCIF1 upregulation in S1HL^{Glu} neurons on the development and maintenance of the SNI-induced nociceptive hypersensitivity using CaMK2α promoter-driven AAV2/9-Pcif1-shRNA (shRNA) strategy (Fig. 2a). As expected, the SNI-induced increase of PCIF1 protein in S1HL from the control Scr-treated SNI mice was not seen in the shRNA-treated mice (Fig. 2b). Notably, SNI-induced mechanical allodynia and heat hyperalgesia were significantly blocked (Fig. 2c–e) or attenuated (Fig. 2f–h) in the shRNA-microinjected mice. Basal responses to mechanical and thermal stimuli on the contralateral side of SNI mice

Fig. 2 | Increased S1HL^{Glu} PCIF1 is required for induction and maintenance of neuropathic pain. a Viral injection schematic and Pcif1-shRNA vector design. **b** S1HL PCIF1 levels significantly decreased 35 days post AAV-CaMK2α-shPcif1 in SNI mice (n = 16 mice). **c**–**e** Pre-injection of AAV-CaMK2α-shPcif1 into contralateral S1HL prevented SNI-induced mechanical allodynia (**c**, **d**) and thermal hyperalgesia (**e**) (n = 10 mice). **f**–**h** Post-injection of shPcif1 reversed established contralateral SNI-induced mechanical allodynia (**f**, **g**) and thermal hyperalgesia (**h**) (n = 8 mice). **i** Experimental timeline in *Pcif1*$^{fl/fl}$ mice. **j** Schematic and images showing reduced PCIF1 in contralateral S1HL^{Glu} neurons after AAV-CaMK2α-Cre injection in *Pcif1*$^{fl/fl}$ mice. Scale bar, 20 μm. **k**, **l** Pre-injection of AAV-CaMK2α-Cre reduced ipsilateral S1HL PCIF1 (**k**, n = 12 mice) and m^{6}Am (**l**, n = 8 mice) levels post-SNI. **m**–**o** Pre-injection of AAV-CaMK2α-Cre prevented SNI-induced mechanical hypersensitivity (**m**, **n**) and thermal hyperalgesia (**o**) (n = 10 mice). **p** Left: Fiber photometry setup for Ca^{2+} imaging in awake *Pcif1*$^{fl/fl}$ mice (drawn by figdraw.com). Right: image shows AAV-CaMK2α-GCaMP6s (Green)/AAV-CaMK2α-mCherry (Red). Scale bar, 500 μm. Heatmaps (**q**), average Ca^{2+} transients (**r**) and AUC quantification of the GCaMP6s signal (3-7 seconds, **s**) from S1HL^{Glu} neurons of *Pcif1*$^{fl/fl}$ mice receiving 0.4 g von Frey stimulation (n = 24 trails from 8 mice). **t** Patch-clamp schematic in S1HL^{Glu} neurons. **u**–**x** Sample traces (**u**), statistical data (**v**), and rheobase of the spike (**w**) for action potential firing and the membrane potential (**x**) recorded from S1HL^{Glu} neurons (n = 13 cells from 4 mice). **e** PWF: paw withdrawal frequencies; PWL: Paw withdrawal latencies. OFT: open filed test; EPM: elevated plus maze; Gs: GCaMP6s. The data are represented as mean ± SEM. S1 samples from two mice were pooled to create one sample (**b**, **l**, **k**). One-way ANOVA followed with Tukey's post hoc test was used for panels (**b**, **k**, **l**, **s** and **v**–**x**). Two-way ANOVA followed with Tukey's post hoc test was used for panels (**c**–**h** and **m**–**o**).

and on either side of the Sham mice were not affected by microinjection of the virus (Supplementary Fig. 2b–g).

Given that shRNA may have potential off-target effects, we generated the *Pcif1*$^{fl/fl}$ mice (Supplementary Fig. 2h, i), in which the endogenous *Pcif1* mRNA in S1HL^{Glu} neurons could be knocked down under the control of the CaMK2α promoter in the presence of Cre recombinase. We found that microinjection of AAV-CaMK2α-Cre (AAV-Cre), not control AAV-mCherry, into the contralateral S1HL 21 days before surgery dramatically reduced the expression of PCIF1 in contralateral (not ipsilateral) S1HL^{Glu} neurons of *Pcif1*$^{fl/fl}$ mice 15 days post-surgery (Fig. 2l–k). Similarly, the SNI-induced elevation of m^{6}Am was also attenuated in the S1HL on day 16 post-surgery in the *Pcif1*$^{fl/fl}$ mice pre-microinjected with AAV-Cre (Fig. 2l). This pre-microinjection also mitigated the SNI-induced pain and anxiety-like behaviors from days 3 to 14 after surgery (Fig. 2m–o; Supplementary Fig. 2j–r).

Given the broad expression of CaMK2α in cortical pyramidal neurons, we utilized Rbp4 (specifically localized to cortical layer 5 excitatory neurons)[42] promoter -driven AAV2/9-Rbp4-Pcif1-shRNA (shRNA) to specifically knock down PCIF1 in the excitatory neurons of S1L5. As expected, the SNI-induced increase of PCIF1 in S1HL was reversed by microinjection of AAV2/9-Rbp4-Pcif1-shRNA on day 21 after treatment, this reversal resulted in the attenuation of nerve injury-induced mechanical allodynia and thermal hyperalgesia (Supplementary Fig. 3a–h). In contrast, microinjection of AAV2/9-Rbp4-Pcif1-shRNA in the motor cortex (M1) slightly decreased PCIF1 level on the contralateral side in both sham and SNI mice, but did not affect the paw withdrawal response to mechanical or thermal stimuli in these animals (Supplementary Fig. 3i–p).

Blocking PCIF1 upregulation in S1HL^{Glu} neurons inhibits the SNI-induced increase in neuronal activity

To examine whether PCIF1 affects the activity of S1HL^{Glu} neurons, we intracranially pre-injected AAV-CaMK2α-GCaMP6s with AAV-Cre or control AAV-eGFP into the S1HL of *Pcif1*$^{fl/fl}$ mice 3 weeks before SNI surgery. We then recorded the GCaMP6s signal, an indicator of Ca^{2+} signaling intensity, from S1HL^{Glu} neurons upon application of a strong mechanical stimulus (0.4 g von Frey filament) to the surgery-side hind paw in the awake mice (Fig. 2p). Mechanical stimulation elicited a significant increase in GCaMP6s signal in S1HL^{Glu} neurons of *Pcif1*$^{fl/fl}$ mice 7 days after SNI in the control eGFP-injected mice. This increase was ameliorated by injection of Cre in S1HL^{Glu} neurons of *Pcif1*$^{fl/fl}$ mice (Fig. 2q–s). Given that the magnitude of the increase in firing rate upon stimulation represents the capacity of the neuronal population in response to input signals, we further examined the activity of S1HL^{Glu} neurons with/without *Pcif1* via whole-cell current clamp recordings in S1HL brain slices obtained 7 days after SNI surgery (Fig. 2t). Consistent with the GCaMP6s fiber photometry results, S1HL^{Glu} neurons in the slices from SNI mice exhibited higher evoked firing rates than those in slices from Sham mice after injection of depolarizing currents (500 ms, 0–200 pA) (Fig. 2u, v). However, no differences were observed in the rheobase of spike and resting membrane potential of S1HL^{Glu} neurons between Sham and SNI mice (Fig. 2w, x). *Pcif1* depletion in S1HL^{Glu} neurons via intracranial pre-injection of AAV-Cre in *Pcif1*$^{fl/fl}$ mice blocked the nerve-injury-induced increase in firing rate in the contralateral S1HL neurons, compared with control injection (Fig. 2v). These results suggest that *Pcif1* is required for the activation of S1HL^{Glu} neurons under neuropathic pain conditions.

Mimicking nerve injury-induced PCIF1 upregulation leads to nociceptive hypersensitivity

To explore whether PCIF1 upregulation in S1HL^{Glu} is sufficient for the initiation of neuropathic pain, we intracranially injected AAV2/9-EF1a-DIO-Pcif1 (DIO-Pcif1) into unilateral S1HL of naïve *CaMK2α-Cre* mice (Fig. 3a, b; Supplementary Fig. 4a). As expected, on day 21 after DIO-Pcif1 injection, the levels of PCIF1 and m^{6}Am were increased by 1.51-flod and 1.512-fold, respectively, compared those after DIO-mCherry (as a control) injection in S1HL (Fig. 3c, d). More importantly, the mice injected with DIO-Pcif1, but not control DIO-mCherry, exhibited the enhanced responses to both mechanical and heat stimuli on the side contralateral to the injection (Fig. 3e–g) and the production of anxiety-like behaviors (Supplementary Fig. 4b–g). Locomotor function is normal in all injected mice (Supplementary Fig. 4c). Spontaneous pain was also observed on day 21 after DIO-Pcif1 injection, as demonstrated by a preference for the chamber paired with lidocaine in the conditioned place preference task (Fig. 3h). These nociceptive-like responses were not seen on the ipsilateral side after injection of DIO-Pcif1 or DIO-mCherry (Supplementary Fig. 4h–j). To further validate this effect, we unilaterally injected AAV-Rbp4-Pcif1 to specifically upregulate PCIF1 in the S1L5^{Glu} neurons of naïve mice (Supplementary Fig. 4k). Overexpression of PCIF1 in S1L5 Rbp4$^+$ neurons significantly led to the development of nociception-like behavior (Supplementary Fig. 4m–r). In contrast, the upregulation of PCIF1 through the injection of AAV2/9-EF1α-DIO-Pcif1 (DIO-Pcif1) in the M1 of *CaMK2α-Cre* mice did not produce enhanced nociceptive responses to mechanical or thermal stimuli (Supplementary Fig. 4s–z). Taken together, these data suggest that upregulation of PCIF1 in S1HL^{Glu} neurons induces neuropathic pain–like symptoms.

PCIF1 upregulation enhances the activity of S1HL^{Glu} neuron

We next sought to determine if PCIF1 upregulation in S1HL^{Glu} neurons could also increase S1HL neuronal activity through measuring GCaMP6s signal (Fig. 3i). We co-injected DIO-GCaMP6s and DIO-Pcif1 (or DIO-mCherry) AAV virus into S1HL of naïve *CaMK2α-Cre* mice 21 days before the experiment. Stimulation with a 0.4 g von Frey filament induced a significantly higher GCaMP6s signal in S1HL from the *CaMK2α-Cre* mice injected with DIO-Pcif1, compared with the *CaMK2α-Cre* mice injected with DIO-mCherry (Fig. 3j–l). In patch clamp studies, further research has revealed that S1HL^{Glu} neurons in slices from DIO-Pcif1-treated mice displayed a significant higher evoked firing rate than S1HL^{Glu} neurons from DIO-mCherry-injected mice (Fig. 3m–o). No

https://doi.org/10.1038/s41467-025-62565-5

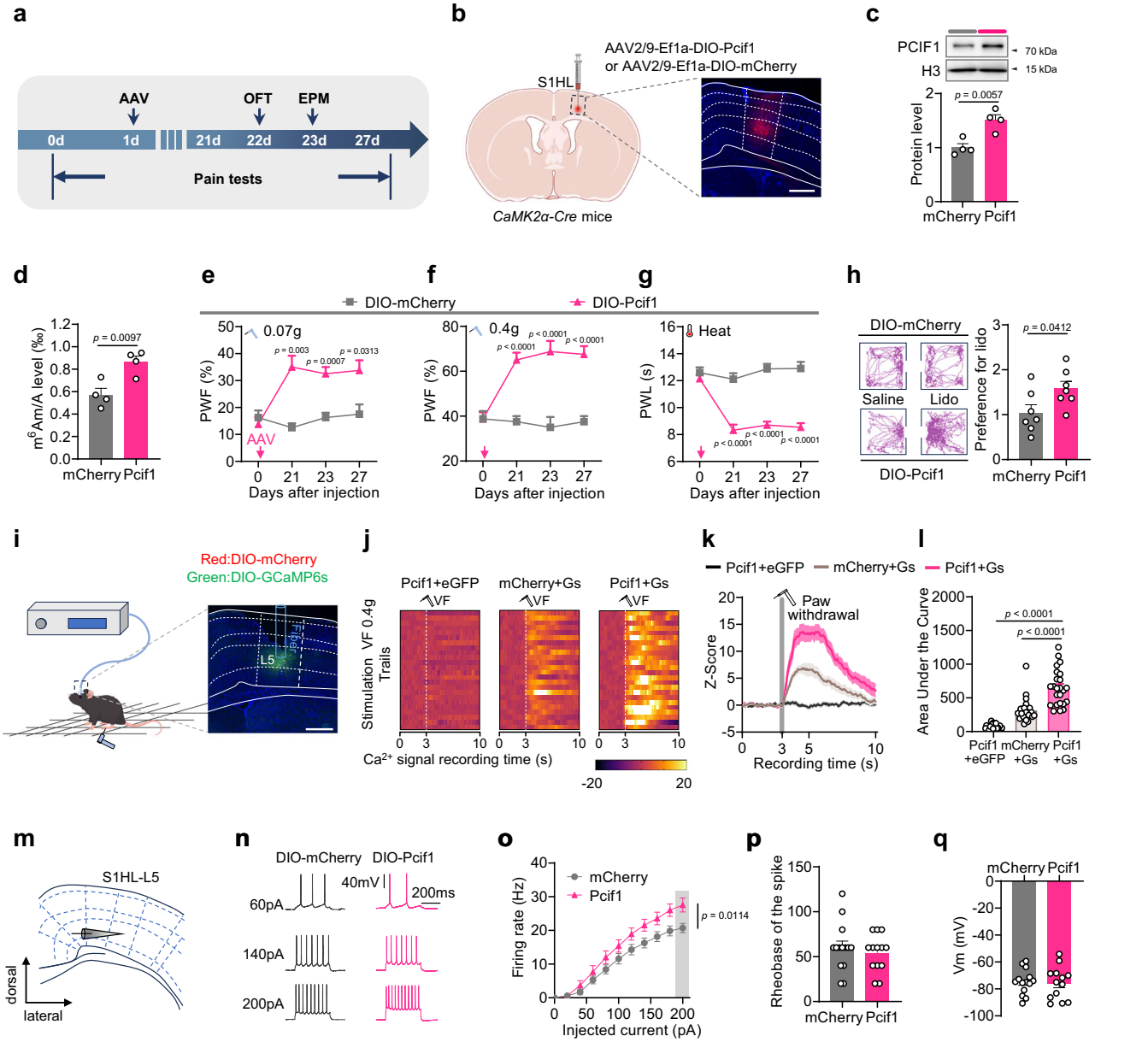

Fig. 3 | Upregulating S1HL^{Glu} PCIF1 induces neuropathic pain- like behavior. **a** Timeline for virus injection and behavior tests in *CaMK2α-Cre* mice. **b** Schematic of the experimental paradigm (left) and a representative image showing mCherry expression in S1HL after injection of AAV-DIO-Pcif1 or AAV-DIO-mCherry into *CaMK2α-Cre* mice (right). Scale bar, 500 μm (left). PCIF1 (**c**) and m^{6}Am (**d**) levels significantly increased 28 days post AAV-DIO-Pcif1 (vs. mCherry) in *CaMK2α-Cre* mice (n = 8 mice). PCIF1 upregulation in S1HL^{Glu} neurons induced contralateral mechanical allodynia (**e**, **f**), thermal hyperalgesia (**g**), as measured by conditioned place preference (**h**) (**e**–**g**: n = 8 mice, **h**: n = 7 mice). **i** Schematic (drawn by fig-draw.com) and image of GCaMP6s recording setup in awake mice (scale bar: 500 μm). Scale bar, 500 μm. Heatmaps (**j**), average Ca^{2+} transients (**k**), and AUC quantification of the GCaMP6s signal (**l**) from S1HL^{Glu} neurons of *CaMK2α-Cre* mice receiving 0.4 g von Frey stimulation (n = 24 trails from 8 mice). **m** Patch-clamp schematic in S1HL^{Glu} neurons. Sample traces (**n**), statistical data (**o**), and rheobase of the spike (**p**) for action potential firings and the membrane potential (**q**) recorded from S1HL^{Glu} neurons in mice with upregulated PCIF1 expression, as described for (**c**, **d**) above (DIO-mCherry group: n = 14 cells from 4 mice, DIO-Pcif1 group: n = 13 cells from 4 mice). The data are represented as mean ± SEM. S1 samples from two mice were pooled to create one sample (**c**, **d**). Student's unpaired t-test (two-tailed) was used for (**c**, **d**, **h**, **p** and **q**). Two-way ANOVA followed with Bonferroni's post hoc test was used for (**e**–**g** and **o**). One-way ANOVA followed with Bonferroni's post hoc test was used for (**l**).

differences in the rheobase of spike and resting membrane potential of S1HL^{Glu} neurons were seen between these two groups (Fig. 3p–q). Thus, PCIF1 upregulation increases the activation of S1HL^{Glu} neurons.

PCIF1 interacts with SERBP1 to catalyze m^{6}Am modification

How does PCIF1 upregulation in S1HL contributes to neuropathic pain? Given that the catalytic activity of epigenetic enzymes often requires the contribution of binding proteins[43], we searched the binding partners of PCIF1 through performing an absolute quantitative LC–MS/MS analysis of the proteins pulled down by endogenous PCIF1 protein, using its specific antibody in human HEK293T and mouse HT22 cells. The approximately 165 and 126 common candidate proteins, respectively, from HEK293T and HT22 cells, were achieved (Supplementary Data 2). Among the candidate proteins, SERBP1 displayed high enrichment in both cells (Fig. 4a; Supplementary Data 2). Although SERBP1 expression were not changed in S1HL days 7 after SNI surgery (Fig. 4b), SERBP1 binding to PCIF1 was increased by 1.49-fold. This increase could be blocked by *Pcif1* knockdown using its shRNA.

https://doi.org/10.1038/s41467-025-62565-5

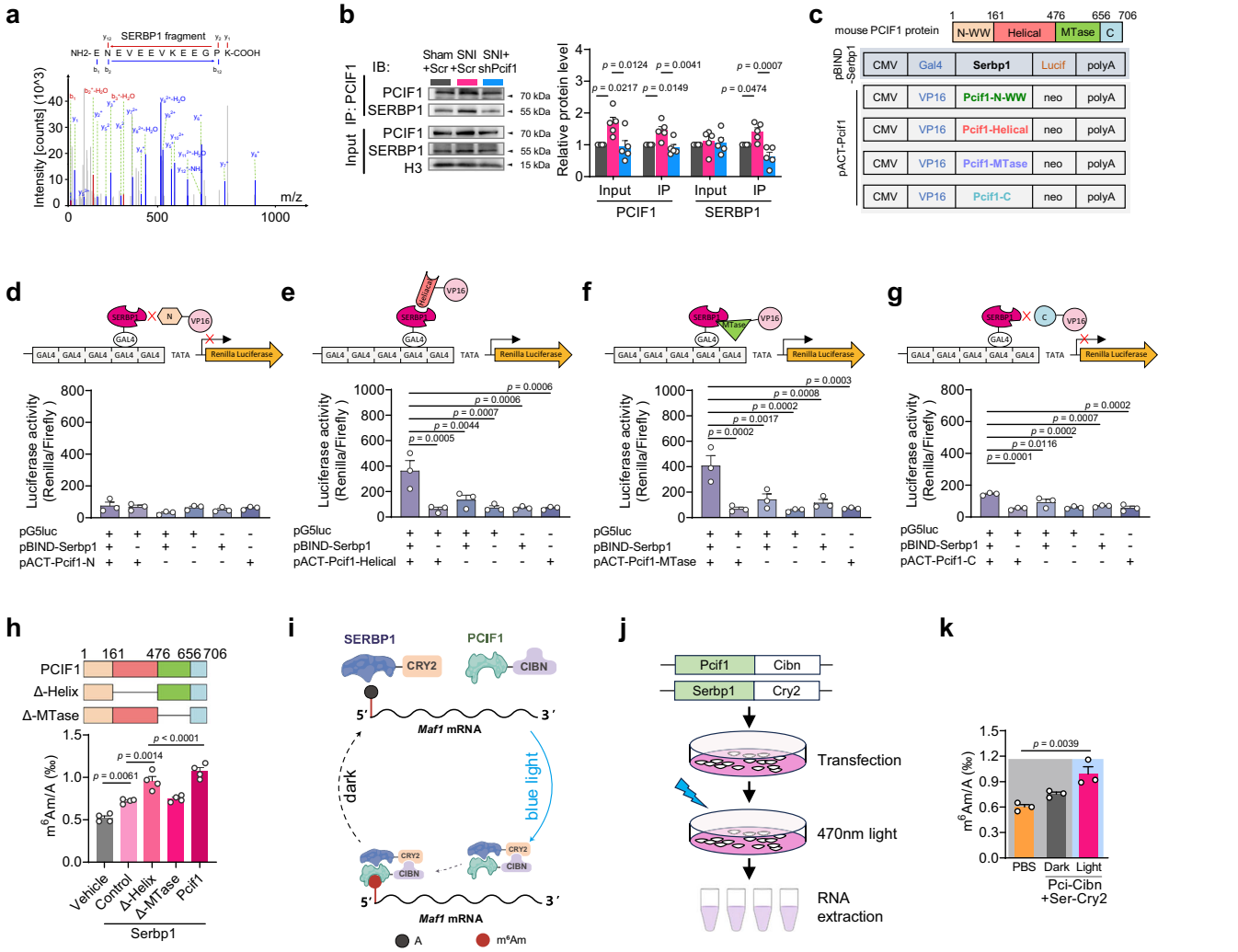

Fig. 4 | SERBP1 and PCIF1 interact and co-catalyze m6Am modifications on mRNA. a The SERBP1 peptide identified by an MS analysis after an anti-PCIF1 co-immunoprecipitation assay in HEK293T cells. **b** Co-immunoprecipitation (IP) analysis of SERBP1 binding to PCIF1, using anti-PCIF1. Tissue was collected from the contralateral S1HL on day 21 after SNI or sham surgery in wild-type mouse pre-microinjected with AAV-CaMK2α-shPcif1 (to knock down *Pcif1* in glutamatergic cells) or a scrambled control. Input, the purified protein control. IB: immunoblotting (n = 10 mice). S1 samples from two mice were pooled to create one sample. **c** Construction schematic for the mammalian two-hybrid system; the luciferase reporter, with full-length Serbp1 and Gal4, and the VP16 transcription factor with a PCIF1 domain. The binding activity of SERBP1 and different PCIF1 domains (N-WW, **d**; helical, **e**; MTase, **f**; C-terminal, **g**) at 48 h after their co-transfection into HEK293T cells (n = 3 dishes of cells). **h** m^{6}Am levels in HT22 cells after 48-hour transfection using: Vehicle (RNase-free water), SERBP1 plasmid with Control (empty vector), SERBP1 with Δ-MTase, SERBP1 with Δ-Helix, or SERBP1 with PCIF1 (n = 4 dishes of cells). **i** Schematic of CRY2/CIBN optogenetic regulation of the m^{6}Am level through control of PCIF1 and SERBP1 binding activity. *Serbp1* and *Pcif1* were fused to the Cry2 and Cibn vectors, respectively. **j**, **k** Diagram showing Serbp1-Cry2 and Pcif1-Cibn co-transfection and activation of their interaction by blue light (**j**), and the quantitation of m^{6}Am levels (**k**) (n = 3 dishes of cells). PBS, transfection of PBS control. The data are represented as mean ± SEM. One-way ANOVA followed with Tukey's post hoc test was used for (**b**). One-way ANOVA followed with Dunnett's post hoc test was used for (**d**–**h** and **k**).

Immunofluorescent staining showed the predominant localization of SERBP1 in the neurons, but not in astrocytes or microglia, in S1HL (Supplementary Fig. 5a, b).

To identify which domain of PCIF1 could interact with SERBP1, we first carried out an in vitro mammalian two-hybridization experiment via constructing report system (Fig. 4c). The reporter was significantly activated after co-transfection of pBIND-Serbp1 with the pACT plasmid containing PCIF1 helical domain or methyltransferase (MTase) domains, but not N terminal domains in HEK293T (Fig. 4d–g; Supplementary Fig. 5c). Although the reporter of the C-terminal domain is activated, the intensity is much smaller than that of the helical domain or MTase domain. This suggests that SERBP1 could interact with the helical and MTase domains of PCIF1.

Next, to investigate whether the interaction between SERBP1 and PCIF1 is essential for m^{6}Am formation. First, we constructed two PCIF1 protein mutants – one lacking the MTase enzyme domain (pCMV-HA-Δ-MTase) and another lacking the Helical domain (pCMV-HA-Δ-Helix). Co-transfection of the pCMV-HA-Δ-MTase plasmid with the pCMV-Serbp1 plasmid resulted in a 3% increase in m^{6}Am levels compared to the co-transfection of the control plasmid with the pCMV-Serbp1 in HT22 cells. In contrast, co-transfection of pCMV-HA-Δ-Helix with pCMV-Serbp1 resulted in a 33% increase (Fig. 4h). These findings indicate that the MTase enzyme domain is required for depositing m^{6}Am in RNA. Moreover, Transfection with pCMV-PCIF1 (CDS full-length expression plasmid) and pCMV-Serbp1 increased m^{6}Am levels by 49% compared to the same controls (Fig. 4h). Based on these findings, we conducted in vitro m^{6}Am catalytic assays to validate the regulatory effects of the SERBP1-PCIF1 complex on RNA m^{6}Am modification. Experimental data revealed that incubation of mRNA with purified SERBP1 protein alone did not alter m^{6}Am levels. Strikingly, co-

https://doi.org/10.1038/s41467-025-62565-5

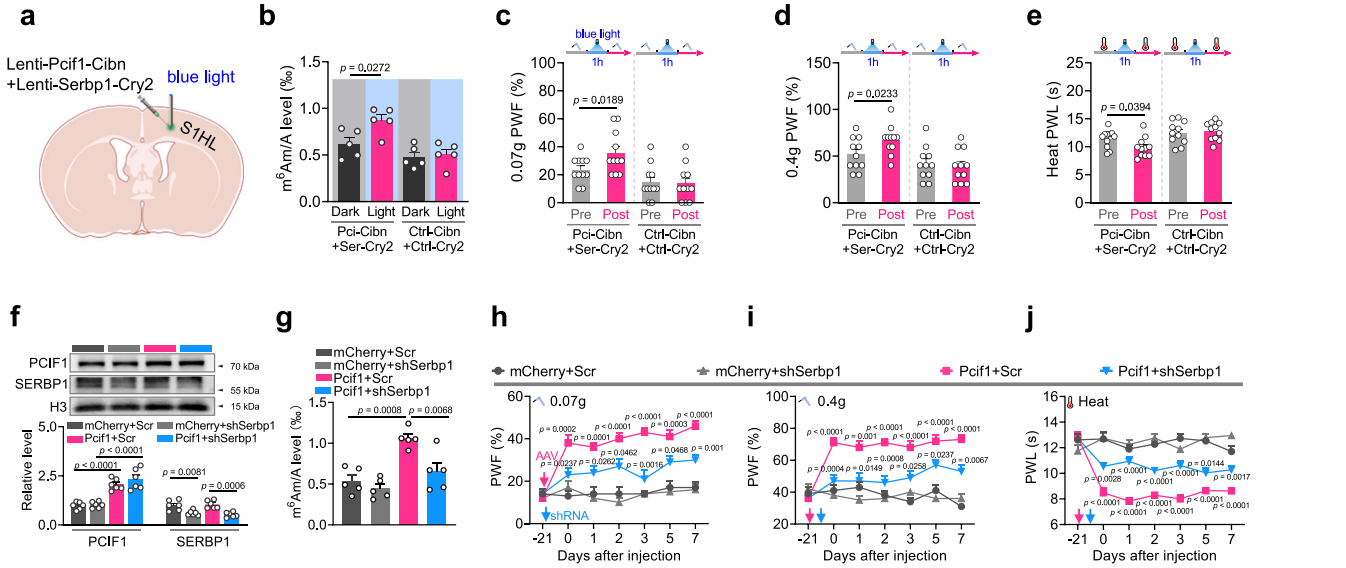

Fig. 5 | The interaction of SERBP1 and PCIF1 contributes to neuropathic pain. **a** Schematic of virus injections and optical fiber implantation for activation of the optogenetic CRY2/CIBN system. **b** m^{6}Am levels at 10 min after 1-h administration of blue light in wild-type mice injected 5 days previously in S1HL with Lenti-Pcif1-Cibn (Pci-Cibn) and Lenti-Serbp1-Cry2 (Ser-Cry2) or their controls Lenti-Cibn (Ctrl-Cibn) and Lenti-Cry2 (Ctrl-Cry2) (n = 10 mice). Pre, Pci-Cibn/Ser-Cry2-injected mice without blue light; Post, Pci-Cibn/Ser-Cry2-injected mice after 1-h blue light. Paw-withdrawal frequencies (PWF) to 0.07 g (**c**) and 0.4 g (**d**) von Frey filaments and paw-withdrawal latencies (PWL) to heat stimuli (**e**) on the contralateral side of mice injected as described in B. Behavioral tests were conducted 10 min after the end of 1 h blue light administration (n = 11 mice). **f**, **g** The level of PCIF1 protein (**f**) and m^{6}Am (**g**) on day 7 after microinjection of AAV-DIO-shSerbp1 (shSerbp1) or AAV-DIO-scrambled-shRNA (Scr) in S1HL of *CaMK2α-Cre* mice preinjected with AAV-DIO-Pcif1 (Pcif1) or AAV-DIO-mCherry (mCherry) (F: n = 12 mice, G: n = 10 mice). Effect of SERBP1 downregulation on the contralateral mechanical (**h**, **i**) and heat (**j**) hypersensitivities induced by PCIF1 upregulation by DIO-Pcif1 (n = 10 mice). Red arrows, DIO-Pcif1 or DIO-mCherry injection. Blue arrows, DIO-shSerbp1 or DIO-mCherry injection. The data are represented as mean ± SEM. S1 samples from two mice were pooled to create one sample (**b**, **f** and **g**). Student's unpaired t-test (two-tailed) was used for (**b**). Student's paired t-test (two-tailed) was used for (**c**–**e**). One-way ANOVA followed with Tukey's post hoc test was used for (**f** and **g**). Two-way ANOVA followed with Tukey's post hoc test was used for (**h**–**j**).

incubation of SERBP1 with purified MTase protein induced a 37% elevation in m^{6}Am level compared to the MTase controls (Supplementary Fig. 5d). These findings suggest that, while SERBP1 is not an essential factor for PCIF1-mediated m^{6}Am methylation catalysis, it significantly enhances the catalytic efficiency of PCIF1 in RNA m^{6}Am modification. To obtain the desired mutant amino acids in SERBP1, we evaluated which amino acids within SERBP1 is crucial for the formation of the SERBP1-PCIF complex. Given that the structure of SERBP1 is unresolved, we combined AlphaFold3 (https://alphafoldserver.com) modeling[44] and alanine-scanning mutagenesis[45] to predict its interaction with PCIF1 and identify potential functional amino acids involved in binding. The prediction results revealed four SERBP1 binding sites on PCIF1, located at amino acid positions 15 (Asn, N), 16 (Arg, R), 21 (Phe, F), and 343 (Asp, D) (the N-terminal amino acid of SERBP1 designated as +1). (Supplementary Fig. 5e, f; Supplementary Table 1). Moreover, to assess the role of these candidate SERBP1 amino acids, we mutated each to alanine and generated individual mutant expression plasmids. LC-MS assay results showed that mutation at position 16 significantly decreased m^{6}Am levels following co-transfection with a *Pcif1* expression vector, compared to the wild-type Serbp1 plasmid (Supplementary Fig. 5g). In contrast, no significant changes in m^{6}Am levels were observed after co-transfection with mutants at positions 15, 21, or 343 and the *Pcif1* expression vector (Supplementary Fig. 5g). These findings indicate that the arginine (R) at position 16 of SERBP1 is essential for its interaction with PCIF1. Together, these findings indicate that the interaction between SERBP1 and PCIF1 is essential for m^{6}Am formation.

To further confirm the role of interaction of SERBP1 with PCIF1 in catalyze m^{6}Am, we employed the CRY2/CIBN optogenetic system, an excellent tool for detecting molecular interactions[46]. SERBP1 and PCIF1 were fused onto the photosensitive proteins CRY2 and CIBN, respectively (Fig. 4j). We hypothesized that the binding of SERBP1 to PCIF1 would be promoted when blue light activated the dimerization of CRY2 and CIBN. As expected, LC–MS showed that, after the application of blue light to HT22 cells co-transfected with Pcif1-Cibn and Serbp1-Cry2 for 48 h, the m^{6}Am level was increased by 1.65-fold (Fig. 4k). Moreover, acute blue light increased the level of S1HL m^{6}Am in naïve mice co-pre-injected with Pcif1-Cibn and Serbp1-Cry2 (Fig. 5a, b). These mice exhibited the enhanced responses to mechanical and heat stimuli on the contralateral side (Fig. 5c–e). Pre-treatment with their controls did not alter basal PWT or PWL on the ipsilateral side (Supplementary Fig. 5h–j). Together, our in vitro and in vivo findings suggest that the interaction between SERBP1 and PCIF1 facilitates m^{6}Am deposition in RNA.

To address whether SERBP1 participates in neuropathic pain and anxiety, we used DIO-Pcif1 and DIO-shSerbp1 AAV virus to respectively upregulate the expression of PCIF1 and downregulate SERBP1 in *CaMK2α-Cre* mice (Fig. 5f). The LC–MS results revealed a strong decline in m^{6}Am in S1HL mRNAs on day 21 after co-injection of DIO-Pcif1 and DIO-shSerbp1 (Fig. 5g), suggesting that knockdown of SERBP1 blocked the increase in m^{6}Am even under the conditions of PCIF1 increase. SERBP1 knockdown in S1HL also ameliorated the contralateral heat and mechanical hypersensitivities induced by S1HL microinjection of DIO-Pcif1 (Fig. 5h–j). As expected, basal PWT and PWL responses were not changed on the ipsilateral side in these mice (Supplementary Fig. 5k–m). Additionally, SERBP1 knockdown in the L5 layer blocked anxiety-like behaviors induced by PCIF1 protein upregulation (Supplementary Fig. 5n–s). Our data strongly support the hypothesis that the contribution of PCIF1 in S1HL to neuropathic pain requires, at least in part, for its binding to SERBP1. Our findings suggest that SERBP1 regulates m^{6}Am methyltransferase activity in vivo.

https://doi.org/10.1038/s41467-025-62565-5

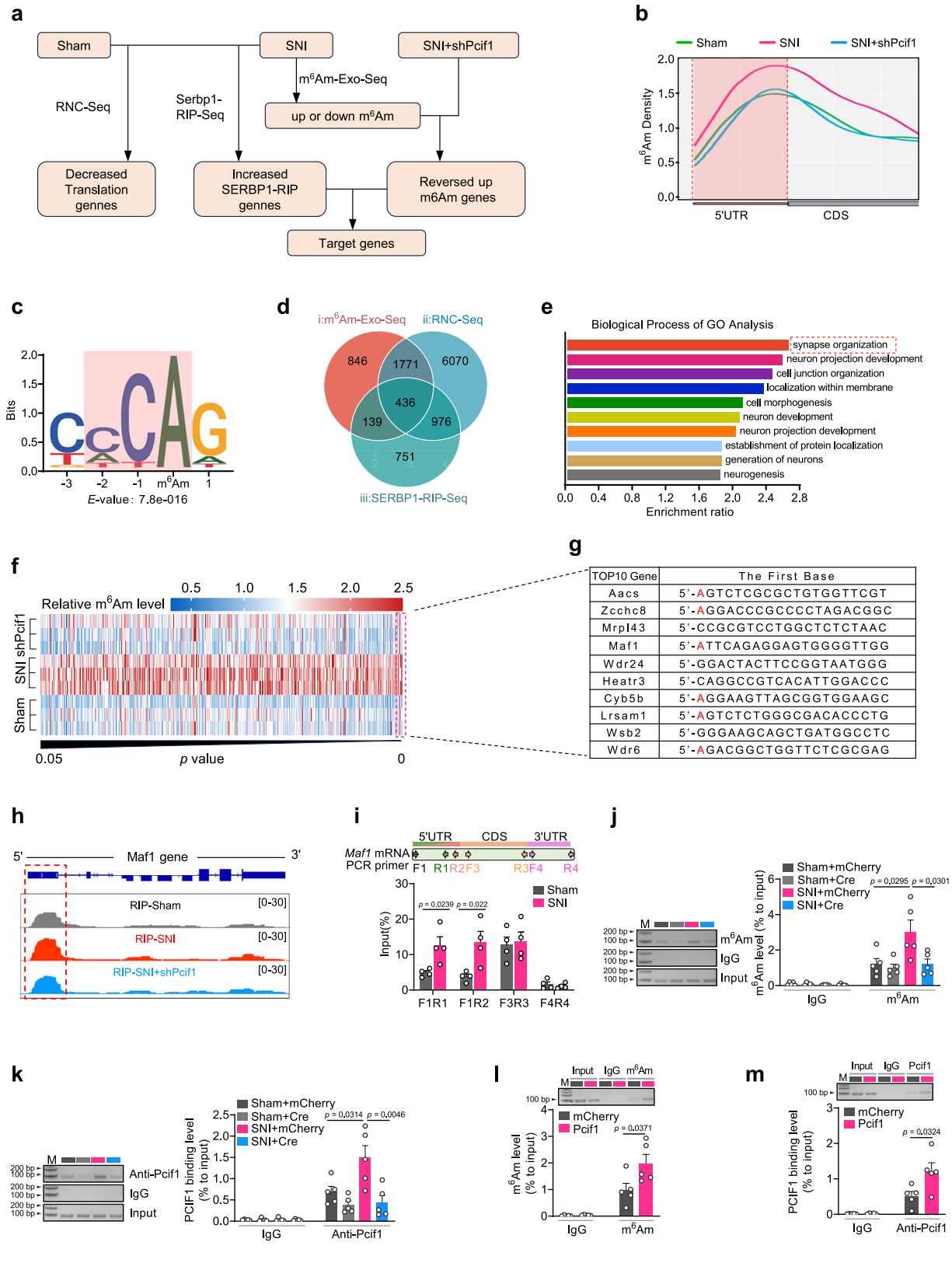

PCIF1 upregulation is responsible for gain of m^{6}Am in *Maf1* mRNA in S1HL after nerve injury

Next, we explored how PCIF1 upregulation in S1HL^{Glu} neurons contributed to neuropathic pain and comorbid anxiety-like behavior. Considering that PCIF1 acts as a "writer" that adds m^{6}Am to the cap site of mRNA, thereby negatively regulating protein translation through its interaction with SERBP1. Therefore, we conducted m^{6}Am mRNA immunoprecipitation sequencing (m^{6}Am-Exo-Seq, Supplementary Fig. 6a) in conjunction with ribosome-nascent chain complex-bound mRNA sequencing (RNC-Seq) and SERBP1 RNA immunoprecipitation sequencing (SERBP1-RIP-Seq) in the S1HL on day 21 post-SNI to identify the downstream targets of PCIF1 (Fig. 6a). About 16,068 genes were identified with m^{6}Am modifications through m^{6}Am-Exo-Seq in sham, SNI, and shPcif1 groups (Supplementary Fig. 6b). The unbiased

Fig. 6 | Increased PCIF1 is responsible for gain of m^{6}Am at *Maf1* mRNA in the S1HL after nerve injury. a Flowchart of the screening for downstream targets of PCIF1 by m^{6}Am-Seq and RNC-Seq. SNI+shPcif1 indicates PCIF1 downregulation in S1HL of SNI mice via injection of AAV-shPcif1. **b** Distribution of m^{6}Am peaks across mRNA segments of S1HL from three groups. **c** Motif analysis of m^{6}Am peaks of mRNAs' genomic sequences. The minus sign in X axis, upstream genomic nucleotides. **d** Venn diagram analysis revealed 436 genes consistently regulated by PCIF1 and SERBP1, based on integrated analysis of three complementary datasets: (i) genes with SNI-induced m^{6}Am increases that were reversed by PCIF1 knockdown (m^{6}Am-Exo-Seq), (ii) genes with increased SERBP1 binding post-SNI (SERBP1-RIP-Seq), and (iii) genes that exhibited reduced translation efficiency following SNI (RNC-Seq). **e** Gene ontology (GO) analysis of biological processes for the 436 genes. **f** Heatmap visualization of *p*-values and fold changes for the 436 genes. **g** Top 10 genes with most significance among 436 genes. **h** The representative image of m^{6}Am peaks on Maf1 gene in S1HL. **i** *Maf1* m^{6}Am in S1HL on day 14 post-SNI measured via RNA immunoprecipitation (RIP)-PCR with four PCR primer pairs. The first two pairs include the RNA cap site (n = 8 mice). The forward F, and reverse R arrows represent paired PCR primers. **j**, **k** *Maf1* m^{6}Am (**j**) and the binding level of PCIF1 to *Maf1* mRNA (**k**) in S1HL of SNI or Sham *Pcif1$^{fl/fl}$* mice after preinjection of AAV-CaMK2α-Cre (Cre) or AAV-CaMK2α-mCherry (Ctrl) into S1HL (n = 10 mice). *Maf1* m^{6}Am level (**l**) and PCIF1 binding to *Maf1* mRNA (**m**) on day 21 after injection of AAV-DIO-Pcif1 or AAV-DIO-mCherry into S1HL of naïve *CaMK2α-Cre* mice (n = 10 mice). For (**i**–**m**), data are represented as mean ± SEM. S1 samples from two mice were pooled to create one sample (**j**–**m**). Student's unpaired t-test (two-tailed) was used for panels (**i**, **j**, **k**). One-way ANOVA followed with Tukey's post hoc test was used for (**l** and **m**).

m^{6}Am-Exo-Seq profiling revealed that m^{6}Am was significantly enriched in the 5′ UTR regions of mRNAs from sham, SNI, and shPcif1 mice (Fig. 6b). Additionally, the genomic sequences surrounding m^{6}Am peaks exhibited a conserved XCA motif pattern (A = m^{6}Am; X = C, G or T) (Fig. 6c), which is consistent with previous reports[47]. The SNI-induced increased m^{6}Am within approximately 3,195 genes was blocked by PCIF1 knockdown (Supplementary Fig. 6c), among which, the translation levels of about 436 genes were reduced and their binding activity to SERBP1 increased after nerve injury (Fig. 6d). These 436 genes may be associated with synaptic organization processes (Fig. 6e). In particular, MAF1, a $GABA_AR$-interacting protein involving in synapse organization, was ranked in top 10 of these 436 genes, and was one of dramatically decreased genes (Fig. 6f, g). Therefore, MAF1 was selected as a candidate target of PCIF1. The SERBP1-RIP-Seq results revealed that SERBP1 bound the mRNAs of about 18,316 genes in the neurons of the sham group, whereas it bound the mRNAs of about 17,773 genes in the SNI group. Further analysis indicated that there were 2238 differential genes between two groups, including Maf1 mRNA (Supplementary Fig. 6d). GO analysis indicates that these differentially genes, including 3195 m^{6}Am-modified genes and 2238 genes bound by SERBP1, exhibit similar enrichment patterns (Supplementary Fig. 6e, f).

Consistent with the previous report[21], the adenosine (A) at the start site of *Maf1* mRNA was methylated with m^{6}Am, and bioinformatics analysis confirmed that *Maf1* mRNA contained a high confident, PCIF1-dependent m^{6}Am site (Fig. 6h). To confirm the *Maf1* m^{6}Am level from m^{6}Am-Exo-Seq, four pairs of primers were designed: the first two pairs (F1R1 and F1R2) covering the 5′UTR region including m^{6}Am site, and the last two pairs (F3R3 and F4R4) covering the CDS and 3′UTR regions (Fig. 6i). We found that F1R1, F1R2, and F3R3 fragments were amplified from the immunoprecipitated m^{6}Am complexes in S1HL tissue lysates. The levels of F1R1 and F1R2 fragments were increased on day 14 after SNI compared with the sham group, where the level of F3R3 fragment was unchanged (Fig. 6i). These observations are consistent with the sequencing results and demonstrates that nerve injury increases the m^{6}Am level of *Maf1* in S1HL. We then examined whether this m^{6}Am gain in *Maf1* mRNA after SNI is caused by PCIF1 upregulation in S1HL neurons. The SNI-induced m^{6}Am increase could be blocked by *Pcif1* knockout in S1HL^{Glu} neurons (Fig. 6j). The PCIF1-RIP assay revealed that the basal binding between the *Maf1* mRNA fragment and PCIF1 was rather weak in sham S1HL. In contrast, there was a striking elevation in the binding activity in S1HL on day 14 after SNI. This elevation was significantly prevented by specific *Pcif1* knockout in S1HL^{Glu} neurons (Fig. 6k). Moreover, PCIF1 overexpression in naïve mice produced an increase in m^{6}Am sites in the *Maf1* mRNA, as evidenced by a 2.09-fold increase in immunoprecipitative activity using the anti-m^{6}Am antibody, compared with the control groups (Fig. 6l). Similarly, the binding of PCIF1 to *Maf1* mRNA was markedly enhanced on day 28 after AAV injection (Fig. 6m). These findings suggest that the SNI-induced gain of m^{6}Am in *Maf1* mRNA can be attributed to the SNI-induced increase in PCIF1 in S1HL^{Glu} neurons.

Furthermore, to assess the effect of SERBP1 on *Maf1* m^{6}Am levels, we assessed the changes in *Maf1* m^{6}Am following SERBP1 knockdown. Similar to PCIF1, the nerve injury-induced increase in m^{6}Am levels of *Maf1* was inhibited by SERBP1 knockdown using its shRNA in S1HL^{Glu} neurons (Supplementary Fig. 6g). Conversely, overexpression of SERBP1 in S1HL^{Glu} neurons of naïve mice resulted in an increase in *Maf1* m^{6}Am levels (Supplementary Fig. 6h). These results suggest that SERBP1 determines the level of m^{6}Am in *Maf1* mRNA.

Increased PCIF1 inhibits MAF1 expression in S1HL after SNI

To determine whether PCIF1 inhibits MAF1 expression in S1HL after SNI, we examined the effect of blocking the nerve-injury induced PCIF1 increase on MAF1 expression. Specific upregulation of *Pcif1* in S1HL^{Glu} neurons in naïve mice by injection of DIO-Pcif1 virus in *CaMK2α-Cre* mice decreased the level of MAF1 protein in the S1HL on day 21 after virus injection (Fig. 7a). Moreover, pre-injection of Cre, but not control mCherry AAV virus, prevented the SNI-induced decrease in MAF1 protein in the S1HL of *Pcif1$^{fl/fl}$* mice on day 21 post-SNI (Fig. 7b). Double-labeled immunostaining revealed that approximately 83.5% of MAF1$^+$ cells in S1HL were co-labeled by NeuN and 5.3% of MAF1$^+$ cells were co-labeled with S100β (Fig. 7c). A subcellular analysis showed that most of the MAF1 staining located in the S1HL neurons (Fig. 7d). Our single-cell RT-PCR assay showed co-expression of *Pcif1* mRNA, *Maf1* mRNA, and *Serbp1* mRNA in 7 of 8 S1HL^{Glu} neurons (Fig. 7e).

Next, to further confirm the specific regulatory role of *Maf1* mRNA m^{6}Am in MAF1 protein expression by PCIF1, we carried out the CRISPR gene-editing system[48]. PCIF1 was fused with inactivated dCasRx protein (dCasRx/PCIF1 fusion protein) to specifically "write" m^{6}Am to the start site "A" in *Maf1* mRNA via guide RNA (gRNA; Fig. 7f). The dCasRx/PCIF1 fusion protein was detectable on day 5 after injection of lentivirus CRISPR-dCasRx-Pcif1 in naïve mice (Fig. 7g). Two gRNAs including gRNA-26 (26 to 44, the first nucleotide in the mRNA designated as +1) and gRNA-60 (60 to 79) located near the 5′UTR region were designed as previously described[38,49]. The m^{6}Am level of *Maf1* was increased by 7.03-fold and 4.87-fold compared to those in the control Scr group on day 5 after co-injection of CRISPR-dCasRx-Pcif1 and gRNA-26 or gRNA-60, respectively (Fig. 7h). Correspondingly, this co-injection significantly reduced the level of MAF1 expression in S1HL by 36% for gRNA-26 and 38% for gRNA-60 on day 5 after injection (Fig. 7i). To further confirm the specificity of CRISPR-dCasRx-Pcif1 with gRNA-26 for *Maf1* mRNA, we tested its effects on *Akt* and *Pik3r1* mRNA. These two genes, identified in our m^{6}Am-Exo-Seq profiles as carrying m^{6}Am modifications, also function as known regulators of Maf1[50,51]. We found no changes in the m^{6}Am levels of *Akt* or *Pik3r1* mRNA, nor in their mRNA levels in S1, after the microinjection of CRISPR-dCasRx-Pcif1 and gRNA-26 (Supplementary Fig. 6i). In contrast, only *Maf1* mRNA showed a significant increase in m^{6}Am following the dCasRx-Pcif1/g26 treatment. Collectively, these results demonstrate that nerve-injury-induced MAF1 downregulation in S1HL results from m^{6}Am elevation via PCIF1.

https://doi.org/10.1038/s41467-025-62565-5

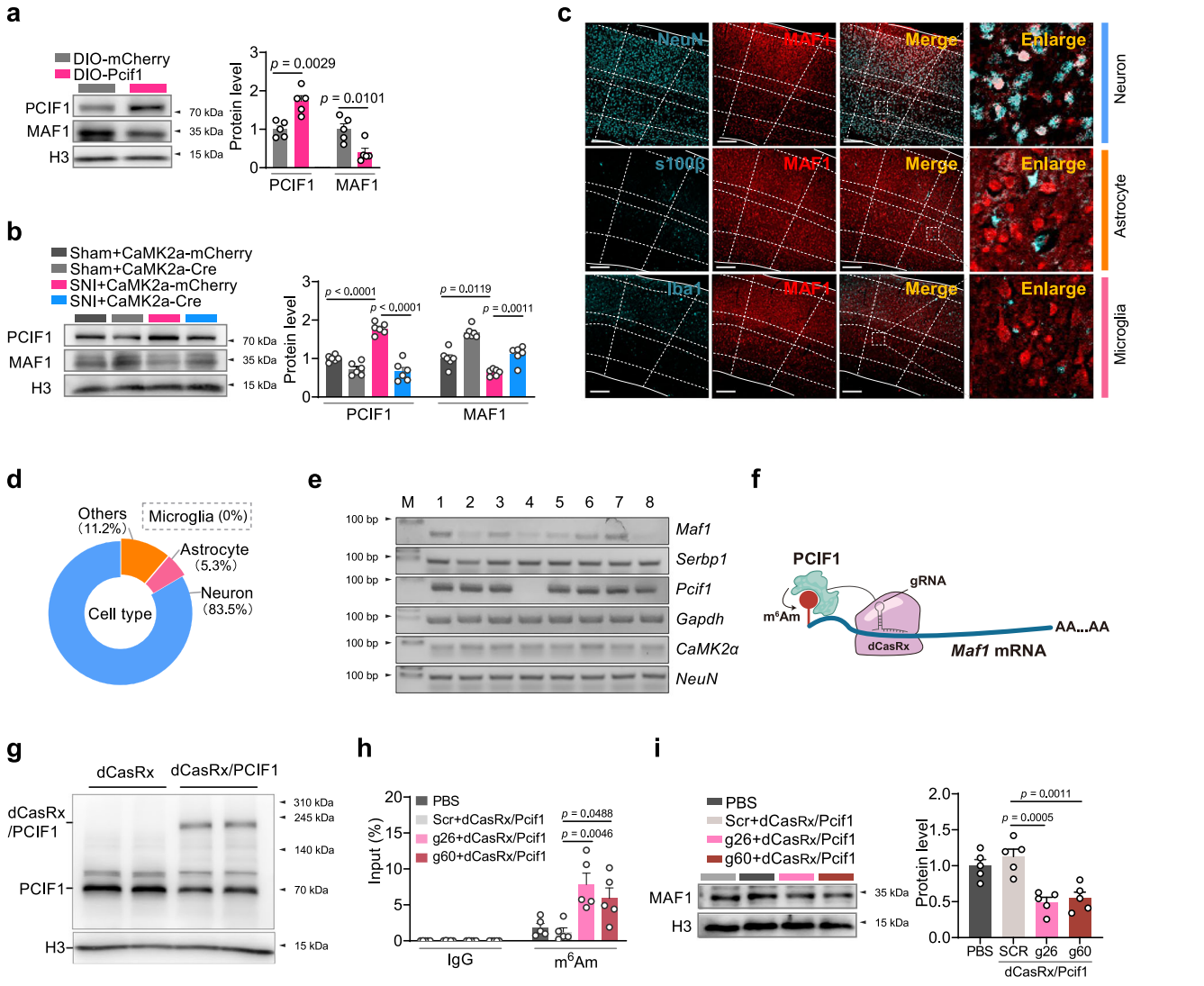

Fig. 7 | Increased PCIF1 leads to SNI-induced downregulation of MAF1 in S1HL. **a** MAF1 protein levels on day 21 after injection of AAV-DIO-Pcif1 (AAV-Pcif1; to induce PCIF1 expression) or AAV-DIO-mCherry (DIO-mCherry) into S1HL of naïve *CaMK2α-Cre* mice (n = 10 mice). **b** The level of MAF1 protein in SNI or Sham *Pcif1*$^{fl/fl}$ mice preinjected with AAV-CaMK2α-Cre (CaMK2α-Cre; to knock out PCIF1) or AAV-CaMK2α-mCherry (CaMK2α-mCherry) into S1HL. Tissue was harvested 21 days after injection (n = 12 mice). **c**, **d** Co-expression analysis of MAF1 (red) with NeuN (a neuronal marker, cyan), S100β (an astrocyte marker, cyan), or Iba1 (a microglia marker, cyan) immunofluorescence staining in the S1HL of naïve mice. n = 4 mice. Scale bar, 200 μm. **e** Co-expression analysis of *Maf1* with *Serbp1* and *Pcif1* in CaMK2α neurons by single-cell PCR. Numbers 1-8 represent eight individual neurons. M, DNA marker. **f** CRISPR-dCasRx/PCIF1 "writing" m^{6}Am to the given site in *Maf1* mRNA. gRNA, small guide RNA. **g** Identification of dCasRx-Pcif1 fusion protein expression on day 5 after microinjection of CRISPR-dCasRx-Pcif1 into S1HL. **h**, **i** The *Maf1* m^{6}Am (**h**) and MAF1 protein (**i**) levels on day 5 after co-microinjection of CRISPR-dCasRx-Pcif1 and gRNA-26 or gRNA-60 into S1HL in naïve mice (n = 10 mice). For (**a**, **b** and **h**, **i**), data are represented as mean ± SEM. S1 samples from two mice were pooled to create one sample (**a**, **b**, **h** and **i**). Student's unpaired t-test (two-tailed) was used for (**a**). One-way ANOVA followed with Tukey's post hoc test was used for (**b**, **h** and **i**).

MAF1 mediates the PCIF1-induced increases in neuropathic pain

We then asked whether *Pcif1*-induced pain and anxiety-like behavior are due to *Maf1* reduction. We first determined whether *Maf1* in S1HL^{Glu} neurons contributes to the neuropathic pain- and anxiety-like behavior. Intracranial injection of DIO-shMaf1 virus decreased the level of MAF1 protein in the S1HL of naïve *CaMK2α-Cre* mice day 28 post-injection (Fig. 8a). This shRNA-caused knockdown of *Maf1* led to hypersensitivity to mechanical and thermal stimuli on the contralateral side (Fig. 8b–d), but not on the ipsilateral side (Supplementary Fig. 7a–c). Additionally, this knockdown also produced the anxiety-like behavior (Supplementary Fig. 7d-i). Moreover, m^{6}Am increase-caused MAF1 downregulation via injection of CRISPR-dCasRx/Pcif1 and gRNA-26 (using same strategy described in Fig. 7f) led to the enhanced behavioral responses (Fig. 8e–g; Supplementary Fig. 7j–r), similar to shRNA effect described above. Injection of DIO-Maf1 virus rescued the SNI-induced decrease in MAF1 in S1HL (Fig. 8h). As expected, this specific rescue ameliorated the SNI-induced nociceptive hypersensitivity (Fig. 8i–k) and anxiety-like responses (Supplementary Fig. 7s–x) on the contralateral side, without affecting basal paw responses on the ipsilateral side of the SNI mice and on either side of the sham mice (Supplementary Fig. 7y–aa). These findings suggest that *Maf1* is responsible for the genesis of neuropathic pain and anxiety behavior after SNI.

Next, we determined the role of *Maf1* in *Pcif1*-induced nociceptive and anxiety-like behavior. Intracranial injection of DIO-Pcif1 AAV virus in S1HL of naïve *CaMK2α-Cre* mice not only increased the level of PCIF1 protein but also decreased the level of S1HL MAF1 expression. However, co-injecting DIO-Maf1 (but not control DIO-mCherry) blocked the

https://doi.org/10.1038/s41467-025-62565-5

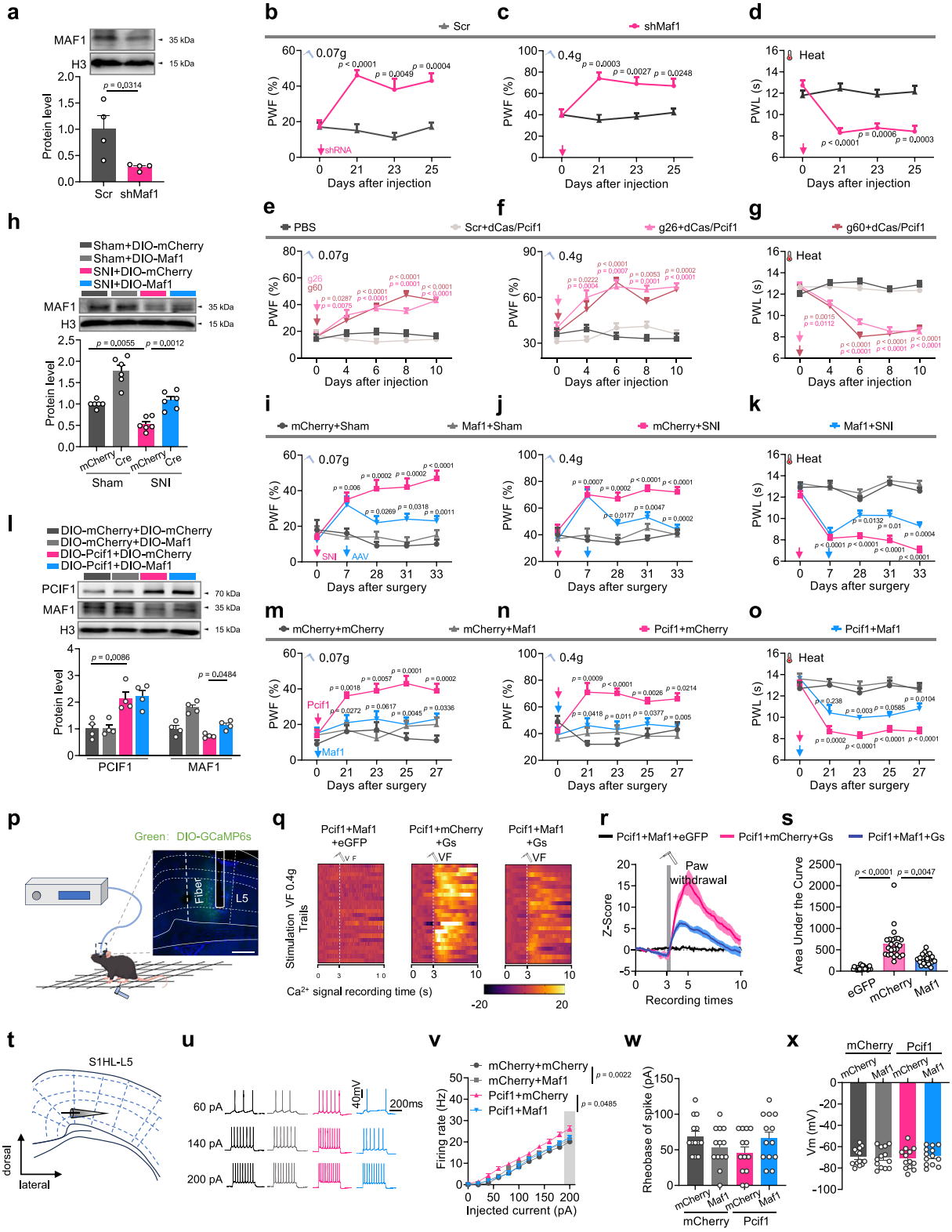

PCIF1-overexpression-induced downregulation of MAF1, without affecting the PCIF1 upregulation caused by DIO-Pcif1 (Fig. 8l). Behaviorally, the enhanced nociceptive responses to mechanical and heat stimuli and anxiety-like behaviors in naïve *CaMK2α-Cre* mice with intracranial injection of DIO-Pcif1 in S1HL were attenuated by MAF1 overexpression caused by co-injecting DIO-Maf1 during the observation period (Fig. 8m–o; Supplementary Fig. 8a–f). Basal behavioral responses on the contralateral side were not affected (Supplementary Fig. 8g–i). Additionally, we explored whether the nociceptive response induced by *Serbp1* upregulation could be blocked by Maf1 overexpression. As expected, intracranial injection of AAV-DIO-Serbp1 produced the augmented responses to mechanical and thermal stimuli in *CaMK2α-Cre* mice. However, these augmented responses were attenuated by the co-injection of AAV-DIO-Maf1 along with AAV-DIO-Serbp1 in these mice (Supplementary Fig. 8j–p). These results suggest that *Serbp1* regulates pain behavior through the mediation of *Maf1*.

Fig. 8 | MAF1 mediates the regulatory effect of PCIF1 on neuropathic pain and comorbid anxiety. a Reduced S1HL MAF1 protein 21 days post AAV-DIO-shMaf1 injection in *CaMK2α-Cre* mice (n = 8 mice). Knockdown of S1HL Maf1 or Co-injection of CRISPR-dCasRx-Pcif1 + gRNA-26/60 induced contralateral mechanical allodynia (**b**, **c**, **e**, **f**) and thermal hyperalgesia (**d**, **g**) (n = 10 mice). **h** MAF1 levels increased after injection of AAV-DIO-MAF1 into *CaMK2α-Cre* mice (n = 12 mice). **i**–**k** Overexpressing MAF1 in contralateral S1HL attenuated SNI-induced mechanical allodynia (**i**, **j**) and thermal hyperalgesia (k) (n = 10 mice). **l** S1HL PCIF1/MAF1 levels after co-injection of AAV-DIO-Pcif1 ± AAV-DIO-Maf1 in naïve *CaMK2α-Cre* mice (n = 8 mice). **m**–**o** MAF1 overexpression blocked PCIF1-induced pain-like behaviors (n = 10 mice). **p** Schematic (left, drawn by figdraw.com) and GCaMP6s expression image (right) for fiber photometry. Heatmaps (**q**), average Ca^{2+} transients (**r**), and AUC quantification (**s**) of GCaMP6s signals recorded from $S1HL^{Glu}$ neurons as mice received 0.4 g von Frey stimulation (n = 24 trails from 8 mice). Scale bar, 200 μm. **t** Schematic of patch-clamp recordings from labeled $S1HL^{Glu}$ neurons in slices. Sample traces (**u**), statistical data (**v**), and rheobase of the spike (**w**) for action potential firing and the membrane potential (**x**) recorded from $S1HL^{Glu}$ neurons (n = 13 cells from 4 mice). Data are represented as mean ± SEM. S1 samples from two mice were pooled to create one sample (**a**, **h** and **l**). Student's unpaired t-test (two-tailed) was used for (**a**) and (**v**). Two-way ANOVA followed with Bonferroni's post hoc test was used for (**b**–**d**). Two-way ANOVA followed with Tukey's post hoc test was used for (**e**–**g**). One-way ANOVA followed with Tukey's post hoc test was used for (**h**, **l**, **s**, **w** and **x**). Two-way ANOVA followed with Tukey's post hoc test was used for panels (**i**–**k** and **m**–**o**).

Together, these findings indicate that MAF1 reduction is necessary for the PCIF1-SERBP1 complex to mediate PCIF1-induced nociceptive and comorbid anxiety-like behaviors.

Upregulation of MAF1 attenuates PCIF1-induced enhancement in Ca^{2+} signal intensity in $S1HL^{Glu}$ neurons

MAF1 is a key player in regulating calcium homeostasis and synaptic remodeling in neurons[52,53]. We finally examined whether upregulating MAF1 blocked the PCIF1-caused enhanced the Ca^{2+} signal intensity. Microinjection of DIO-GCaMP6s plus DIO-Pcif1 AAV virus (but not control DIO-mCherry) into S1HL of naïve *CaMK2α-Cre* mice led to a significant increase of GCaMP6s signal in response to 0.4 g von Frey filament stimulation, as measured on day 27 post-injection (Fig. 8p–s). This increase was markedly reduced by co-injection of DIO-Maf1. Notably, patch-clamp electrophysiological analyses revealed that *Maf1* knockdown significantly increased action potential firing rates in pyramidal neurons (Supplementary Fig. 8s). Conversely, *Maf1* overexpression completely abolished the PCIF1-mediated enhancement of neuronal excitability (Fig. 8v). These data suggest that MAF1 also participates in the process by which PCIF1 regulates neuronal activity in S1HL.

Discussion

Epitranscriptomic modifications have recently emerged as a focal point in chronic pain research due to their extensive regulatory effects on gene expression[54]. As one of the most prevalent RNA modifications, m^6Am and its methyltransferase PCIF1 have been shown to involve in many biological processes and human diseases[19,23,55–57]. Bioinformatic analyses of m^6Am profiling from 45 human and 16 mouse tissues have indicates that m^6Am is brain tissue-specific[58]. Human and mouse m^6Am modifications are often dysregulated in nervous-system-related diseases[59], but it remains unclear exactly how m^6Am is involved in brain-associated physiological and pathological functions. In the present study, we reported that an interaction between SERBP1 and PCIF1 after peripheral nerve injury contributes to deposition of m^6Am on mRNA in the primary somatosensory cortex (S1). Furthermore, we demonstrated that the SERBP1–PCIF1 interacting complex in S1HL participates in the initiation and maintenance of neuropathic pain and anxiety-like behavior via targeting of m^6Am to *Maf1* mRNA. Our study provides the evidence to support a functional role for m^6Am and its methyltransferase in the genesis of neuropathic pain and comorbid anxiety and indicates potential therapeutic strategies for the treatment of these disorders.

Several recent single-cell RNA sequencing reports showed that *Pcif1* mRNA is expressed in the nervous system, including in S1 of mouse and macaque[60,61]. Immunofluorescence in vitro assays revealed that PCIF1 is localized predominantly in the nucleus in the cancer cells HCT116 and HT29 CRC[26]. Interestingly, an in vitro study reported that PCIF1 is enriched in both the nucleus and the cytoplasm in neck squamous cells[23]. Here, we found that PCIF1 was localized mainly in the nuclei of adult mouse S1 cortical neurons, consistent with the previous in vivo observations[26]. Neuronal distribution pattern of PCIF1 in S1 cortex suggests its potential role in nociceptive sensation and emotion processing.

Neuropathic pain is a common health problem, but its treatment is severely limited, partially because the molecular mechanisms underlying this disorder remain elusive. We here showed PCIF1 upregulation in S1 cortex in the preclinical mouse model of neuropathic pain with comorbid anxiety caused by peripheral nerve injury (SNI, CCI), diabetes, and chemotherapy, but not in the preclinical mouse model of chronic inflammatory pain or chronic restraint stress (to induce anxiety alone). These data strongly suggest that the upregulation of S1 PCIF1 is specific to neuropathic pain. Additionally, our findings support previous conclusions indicating that distinct mechanisms are involved in anxiety disorders compared to those induced by neuropathic pain[62].

Importantly, the upregulation of PCIF1 occurred specifically in $S1HL^{Glu}$ neurons. A previous reports showed that peripheral nerve injury increased hyperactivity of S1HL pyramidal neuron[35]. We further showed that PCIF1 upregulation in $S1HL^{Glu}$ contributed to the development and maintenance of neuropathic pain and comorbid anxiety, demonstrated by the attenuation of nociception and anxiety-like behaviors and by the amelioration of enhanced Ca^{2+} signaling and $S1HL^{Glu}$ neuronal excitability after specific knock-down or conditional knock-out of PCIF1 in $S1HL^{Glu}$ in SNI mice. Thus, PCIF1 in $S1HL^{Glu}$ is likely a key initiator of neuropathic pain and comorbid anxiety.

The SERBP1–PCIFI complex is required for the increased deposition of m^6Am in mRNA in $S1HL^{Glu}$ neurons in SNI mice. Co-factors are known to contribute to process by which methyltransferases deposit modifications onto mRNA[63,64]. For instance, Wilms' tumor 1–associating protein (WTAP) is a co-factor of METTL3, as their protein complex catalyzes the RNA m^6A modification[43]. However, the mechanism underlying PCIFI deposition of m^6Am onto mRNA is poorly understood. In this study, we demonstrate that SERBP1 interacts with PCIF1 to regulate m6Am deposition on mRNA, and that arginine residues at position 16 of SERBP1 are essential for this interaction. Indeed, SERBP1 is a well-known regulator of Serpine1 mRNA stability[29], and was recently reported to have chaperone-like properties incell metabolism and histone methylation[65–67]. In addition, SERBP1 has a central role in brain function and development, especially neurogenesis and synaptogenesis[30–32]. SERBP1 is frequently localized in the cytoplasm and the nucleus because of the level of arginine methylation in the C-terminal region[68,69]. Consistently, the present study showed that SERBP1 was localized in both nucleus and the cytoplasm of S1HL neurons, where it plays a crucial role in the activity of PCIF1 and catalyzation of m^6Am formation. We used a CRY2/CIBN optogenetic system to enhance SERBP1 binding to PCIF1. This binding resulted in an increase in the total level of m^6Am in S1, as well as in nociceptive and anxiety-like behaviors. Notably, we successfully constructed the lentiviral vector Lenti-PCIF1-Cibn to overexpress PCIF1. However, due to the limitations of viral expression efficiency and vector capacity, this system resulted in only a modest 29% increase in m^6Am levels. Even

this slight increase seems sufficient to trigger mild pain-like behavioral manifestations in dark conditions. The identification of SERBP1 as a cofactor of PCIF1 represents a significant finding. This discovery is particularly important considering the ongoing challenges in understanding the mechanisms by which epigenetic modification proteins, including DNMTs, METTL3, NAT10, and PCIF1 deposit various epigenetic modifications, particularly the recently discovered m^6A, m^6Am, and ac^4C modifications in DNA or RNA.

PCIF1 catalyzes m^6Am methylation only at 5′ terminal of capped mRNAs, not within internal m^6A methylation. Our m^6Am-Seq assay revealed that many transcripts gained m^6Am in contralateral S1 after nerve injury, and these gains correlate with the SNI-induced elevation in S1 PCIF1. SNI led to the changes in m^6Am modification in many mRNAs, including both increases and decreases of m^6Am levels in certain mRNAs. Unlike PCIF1, the expression of FTO, a known demethyltransferase of m^6Am, was not altered in S1 after SNI. Which proteins are responsible for erasing the m^6Am modification in mRNAs? Future studies will be necessary to address these questions. Peripheral nerve injury increased the level of m^6Am level, but decreased the level of m^6A, in S1. The abundance and alteration between m^6Am and m^6A do not appear to be correlated, consistent with previous findings[58]. As m^6Am is adjacent to m^7G in mRNA[19,20], here, we found m^7G was also increased in S1 under conditions of neuropathic pain. Whether their adjacent location is linked to this consistency remains to be determined.

MAF1 may participate in the role of PCIF1 in neuropathic pain and associated anxiety occurs. Blocking PCIF1 expression by microinjection of AAV-Cre virus into SNI *Pcif1*$^{fl/fl}$ mice or AAV-Pcif1-shRNA in SNI mice blocked the increases in *Maf1* m^6Am, rescued the decreased expression of MAF1 protein in S1 cortex, and blocked the development of neuropathic pain and associated anxiety. Mimicking nerve-injury-induced PCIF1 upregulation through S1HL injection of DIO-Pcif1 AAV virus in naïve *CaMK2α-Cre* mice increased *Maf1* m^6Am, reduced MAF1 protein expression in S1, and augmented the animals' nociceptive and anxiety-like responses. Furthermore, we used the CRISPR-dCasRx system to show that PCIF1 has a direct effect on MAF1 expression in a *Maf1* m^6Am-dependent manner[38,70–73]. It is well documented that MAF1 is an endogenous regulator of neuronal excitability in optic neuropathy, learning and memory disorders, Alzheimer's disease, and ischemic stroke[52,74–76]. MAF1 enhances $GABA_AR$ receptor activity, and thus has an inhibitory effect on neural activity[53]. The anti-nociceptive effect of reversing PCIF1 upregulation in SNI mice is likely due to rescue of the reduction in MAF1 expression. In line with this, PCIF1 upregulation enhanced stimulus-evoked calcium activity in $S1HL^{Glu}$ neurons, and this enhancement was blocked by overexpression of MAF1 in $S1HL^{Glu}$ neurons. However, we cannot rule out other mechanisms through which PCIF1 may be involved in neuropathic pain and associated anxiety. Our RNC- and m^6Am-sequencing analyses revealed that, in addition to *Maf1*, changes in other genes such as *Aacs* and *Zcchc8* were also identified following SNI, which could potentially contribute to m^6Am-mediated modulation of neuropathic pain via distinct pathways. Whether these genes also mediate the role of PCIF1 in neuropathic pain and associated anxiety remains to be further investigated. In addition, sex dimorphism in pain and anxiety is a well-recognized clinical phenomenon[77,78]. As this study primarily used male mice, whether the above mechanisms are male-specific remains unclear. We will examine these mechanisms in mice in future studies.

In summary, we have demonstrated that SERBP1 acts as a cofactor of PCIF1, and that the SERBP1–PCIF1 complex is essential for catalyzing m^6Am modification. Blocking the nerve-injury-induced increase in $S1HL^{Glu}$ SERBP1–PCIF1 mitigated neuropathic pain and alleviated anxiety-like behaviors, without impairing of locomotor function. The effects of the SERBP1–PCIF1 complex on neuropathic pain occur, at least in part, through the m^6Am modification of *Maf1* in S1, leading to a reduced expression of MAF1 and an increase in neuronal excitability in the S1 cortex. (Fig. 9). This study establishes the initial link between RNA m6Am and neuropathic pain, along with associated comorbid anxiety. Our study suggests that the SERBP1–PCIF1 complex may be a potential clinical target for the management of this disorder.

Methods

Animals

Healthy male and female BALB/c and C57BL/6 mice were obtained from Xuzhou Medical University. *CaMK2α-Cre*, *Pcif1*$^{fl/fl}$ and *tdTomato*$^{fl/fl}$ mice were purchased from Cyagen Biosciences. *vGat-Cre* mice were purchased from Shanghai Model Organisms Center, Inc. Mice were housed in standard conditions (Specific Pathogen-Free facility, 12 h light/dark cycle, temperatures of 23 ± 3 °C and humidity of 30–60%), with ad libitum access to food and water. All animal procedures were performed in accordance with protocols approved by the Institutional Animal Care and Use Committee of Xuzhou Medical University (the protocol number: 202207S038). BALB/c mice were used for preliminary validation of the viral construct. C57BL/6 mice were employed in all experiments except the preliminary viral construct validation. Female mice were used exclusively to examine the effect of sex on PCIF1 expression in the S1HL after SNI, and other experiments employed male mice. For each experiment, the animals were randomized to either the control or the experimental group. All efforts were made to minimize animal suffering and to reduce the number of animals used.

Mouse genotyping

CaMK2α-Cre, vGat-Cre, tdTomato$^{fl/fl}$ and *Pcif1*$^{fl/fl}$ mice were identified by genotyping. A small mouse tail sample was collected, and DNA was extracted using the phenol-chloroform method. PCR analysis was performed to identify wild-type and mutant mice. PCR amplification was conducted using 500 ng of DNA in a 20 μL reaction volume, containing 10 μL of 2× Taq PCR MasterMix (Vazyme, China) and 1 μL of 10 μM primers. The primer sequences used in these reactions can be found in Supplementary Data 1. DNA and primers were denatured at 94 °C for 3 min, followed by 35 cycles of 94 °C for 30 s, 60 °C for 35 s, and 72 °C for 55 s, with a final extension at 72 °C for 5 min. Amplicons were separated using a 1.5% agarose gel and imaged with the Uvitec System (Q9 Alliance, Uvitec).

Animal models

Four peripheral nerve injury-induced neuropathic pain models—spared nerve injury (SNI)[79], chronic constriction injury (CCI)[80], diabetic neuropathic pain (DNP)[81], and chemotherapy-induced neuropathic pain[82]—were prepared for experiments. For the SNI model, mice were anesthetized with 2% isoflurane. The left sciatic nerve was exposed and the common peroneal and tibial nerves were loosely ligated with nonabsorbent 5-0 chromic gut sutures. Subsequently, 1 mm sections distal to the sutures were removed, while the sural nerve was left intact. The pre-treatment of CCI model was similar to that in SNI model. After exposing the left sciatic nerve, three loose straps of 4-0 silk thread were placed around the sciatic nerve at intervals of about 1 mm at the proximal end of the trigeminal nerve.

For DNP model, mice were randomly assigned to either a normal chow diet (ND) group or a high-fat diet (HFD) group. After 4 weeks, citrate buffer solution was injected intraperitoneally into ND mice once a day for 3 days, while streptozotocin (STZ, 30 mg/kg, Beyotime) was injected into HFD-fed mice. Mice were evaluated according to the following criteria[1]: fasting glucose levels exceeding 16.7 mM[2]; elevated food and water consumption, increased urine output, and weight loss.

For chemotherapy-induced neuropathic pain model, cisplatin (2.3 mg/kg/day; MedChemExpress) or phosphate buffered saline (PBS) was injected intraperitoneally for two cycles of five daily injections

https://doi.org/10.1038/s41467-025-62565-5

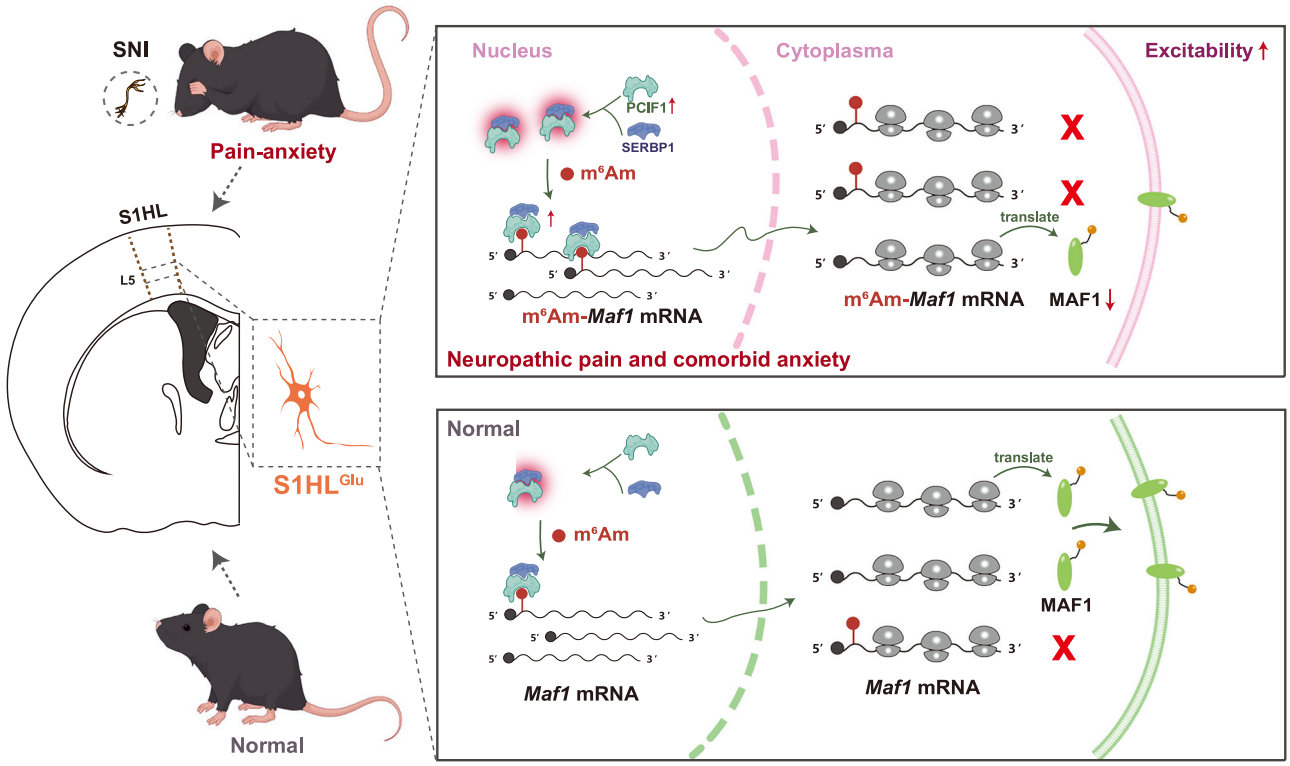

Fig. 9 | Cartoon showing the mechanism by which the SERBP1-PCIF1 complex in S1HL^{Glu} neurons contributes to the development and maintenance of neuropathic pain and comorbid anxiety. Peripheral nerve injury induces an increase in the SERBP1-PCIF1 complex, which in turn regulates m^{6}Am-controlled MAF1 expression in S1HL, leading to reduced inhibition and enhanced neuronal excitability (drawn by figdraw.com).

followed by 5 days of rest. Mice were observed carefully for any abnormal behavioral changes every day after treatment.

Chronic restraint stress (CRS)[34] is a common mouse model of anxiety/depression. Mice were placed in a well-ventilated 50 mL centrifuge tube for 2 h daily (10:00 a.m. to 12:00 p.m.) over 7 consecutive days. The control group received no treatment. Anxiety-like behavior was evaluated on the 8th day using the elevated plus maze and open field test.

Tissue collection

To ensure the reproducibility of the experiments, we designed rigorous methods to collect S1HL. Mice were anesthetized, euthanized, and immediately perfused with PBS through the heart left ventricle before the brains were removed. The brain was then placed in a rodent brain matrix (ST-1175, TOW-INT TECH). Coronal sections (500 μm) were cut using razor blades, and the slices were transferred to ice-cold PBS. According to the mouse brain atlas (second edition), the S1HL tissue was dissected using a razor blade and curved forceps under a stereomicroscope. The specific location of S1HL varies across different brain slices. The corresponding S1HL location was confirmed based on the morphology of the corpus callosum, the commissure, the lateral ventricle, and the hippocampal fimbria. The S1HL tissues were collected from Bregma: 0.38 to −0.22 mm.

Stereotaxic viral injections

Mice were anesthetized with isoflurane (2%) and immobilized on a stereotaxic device. Virus was injected into the brain (infusion speed 0.1 μl/min) with a Hamilton syringe containing a 33-gauge stainless steel needle connected to a stereotaxic infusion pump. The coordinates used to target the S1HL/S1L5 area was as follows: AP: −0.5 mm, ML: −1.7 mm, DV: −1.3 mm; that to motor cortex (M1) area was as follows: AP: −0.22 mm, ML: -1.0 mm, DV: −1.3 mm. The needle was left in place for 5 minutes after the injection to prevent backflow. After injection, the animals were placed in a clean cage, and the cage was kept warm until full recovery from anesthesia.

The AAV-CaMKIIα-shPcif1-WRPE (AAV2/9, 5.3×10^{12} vg/mL), AAV-CaMKIIα-Scr-WRPE (AAV2/9, 5.1×10^{12} vg/mL), AAV-Ef1α-DIO-Pcif1-mCherry (AAV2/9, 7.3×10^{12} vg/mL), AAV-Ef1α-DIO-mCherry (AAV2/9, 4.9×10^{12} vg/mL), AAV-RBP4-Pcif1-eGFP (AAV2/9, 8.6×10^{12} vg/mL), AAV-RBP4-shPcif1-eGFP (AAV2/9, 3.8×10^{12} vg/mL), AAV-RBP4-eGFP (AAV2/9, 6.5×10^{12} vg/mL), AAV-RBP4-Scr-eGFP (AAV2/9, 5.7×10^{12} vg/mL), Lenti-Pcif1-Cibn (8.0×10^{9} VP/mL), Lenti-Serbp1-Cry2 (1.3×10^{9} VP/mL), AAV-Ef1α-DIO-Serbp1-mCherry (AAV2/9, 3.3×10^{13} vg/mL), AAV-CaMKIIα-shSerbp1-WRPE (AAV2/9, 6.9×10^{12} vg/mL), AAV-Ef1α-DIO-Maf1-mCherry (AAV2/9, 5.2×10^{12} vg/mL), AAV-CaMKIIα-shMaf1-WRPE (AAV2/9, 1.6×10^{13} vg/mL) were generated through a systematic process involving vector construction and viral packaging. AAV-CaMKIIα-Cre (AAV2/9, 5.7×10^{12} vg/mL), AAV-CaMKIIα-GCaMP6s (AAV2/9, 6.1×10^{12} vg/mL) and AAV-hSyn-DIO-GCaMP6s (AAV2/9, 6.7×10^{12} vg/mL) were purchased from Obiosh Biotechnology (Shanghai, China).

Behavioral tests

Paw withdrawal frequency (PWF) and paw withdrawal latency (PWL) were measured to assess mechanical and thermal pain sensitivity[38]. Paw withdrawal frequencies (PWFs) in response to mechanical stimuli were measured using two calibrated von Frey filaments (0.07 g and 0.4 g, Stoelting Co.). In brief, the tested mouse was placed in a Plexiglas chamber to habituate for 30 min. The 0.07 g and 0.4 g von Frey filaments were applied to the plantar surface of each hind paw for 1 second, repeated 10 times at 5-minute intervals. The PWF was calculated as the percentage of positive responses among the 10 applications, using the formula: (number of paw withdrawals/10 trials) × 100. Paw withdrawal latencies (PWLs) were evaluated by recording the time

taken to withdraw the hind paw in response to heat stimulation using the Model 336 Analgesia Meter, Series 8, IITC Life Science. Briefly, the tested mouse was placed in an individual Plexiglas cage on a glass plate. A beam of noxious light was directed at the center of each hind paw's plantar surface. The PWL was measured as the interval from the initiation of the light beam to the hind paw withdrawal. The test was conducted five times at 5 min intervals per side. A 20 s cutoff time was implemented to prevent tissue injury.

Modified conditioned place preference (CPP) paradigm was employed to evaluate spontaneous pain behaviors in mice[83]. Mice were briefly placed in an apparatus consisting of two Plexiglas compartments connected by a tunnel. Compartment 1 featured a rough floor and walls adorned with horizontal black-and-white stripes. Compartment 2 featured a smooth floor and walls adorned with vertical black-and-white stripes. The time spent in each compartment was automatically recorded by the MED-PCIV CPP software. Initially, mice were preconditioned for 30 minutes with access to both compartments to familiarize them with the environment. Post-preconditioning phase, data analysis within 15 minutes assessed preexisting compartment bias in mice. Further testing was not performed on mice that spent over 80% or less than 20% of the total time in any one compartment. The connecting tunnel was closed for the next 3 days during the conditioning protocol. Mice were intrathecally injected with saline (5 μl) and then allowed to habituate for 15 min in the saline-paired compartment. Six hours later, 5 μl of 0.8% lidocaine in saline was injected intrathecally and paired with the opposite conditioning compartment. On the test day, the mice were placed in the connecting tunnel and explored both compartments freely for 15 min. The CPP score was defined as the test time spent in the lidocaine chamber divided by the preconditioning time spent in the lidocaine chamber.

The elevated plus maze (EPM) and open field test (OFT) were employed to assess anxiety-like behaviors in mice[84]. The EPM consisted of four 30 cm × 6 cm arms (two closed arms and two open arms) and a central 6 cm × 6 cm platform. Mice were placed in the center of the apparatus and allowed to move freely. The number of entries and time spent in each arm was recorded by ANY-maze software (Stoelting Co). OFT was performed in a square arena (50 × 50 × 30 cm). The arena was evenly divided into 25 small squares (10 cm × 10 cm), with the central 9 squares defined as the central zone and the outer 16 squares defined as the peripheral zone. The mice were placed into the central zone of the apparatus and allowed to freely explore the arena for 10 min. The time spent in the center and the total movement distance were recorded by ANY-maze software.

RNA extraction and quantitative real-time polymerase chain reaction

Quantitative real-time PCR (qRT-PCR) was performed to determine mRNA expression levels[85]. To reverse transcribe into cDNA, 400 ng RNA was extracted from $S1HL^{Glu}$ neurons with RNAiso reagent (9109, Takara). RT–qPCR was performed with 2× SYBR Premix ExTaqII (RR820A, Takara) and run on a LightCycler480. PCR cycling conditions were performed at 95 °C for 5 min, followed by 40 cycles of 95 °C for 10 s, 60 °C for 20 s, and 72 °C for 30 s. All RT–qPCR primer sequences are listed in Supplementary Data 1.

Single-cell RT-PCR

CaMK2α-Cre and *vGat-Cre* mice were crossed with $tdTomato^{fl/fl}$ mice to label CaMK2α neurons and GABA neurons, respectively, in the nervous system. After genotyping the offspring, CaMK2α-td and vGat-td mice at 8 weeks of age were subjected to SNI or Sham surgery. On 21 days post-surgery, pain hypersensitivity was validated, and S1HL brain slices were prepared according to the brain slice electrophysiology protocols. Glass pipettes with appropriate tip diameters were pulled and used to approach the S1HL region under an inverted phase-contrast microscope. Fluorescently labeled neurons were aspirated into the pipette via gentle suction. The pipette was quickly removed from the solution, and its contents including the cell and surrounding fluid were expelled into a nuclease-free PCR tube containing 10 μL of cDNA lysis buffer. The samples were stored at −80 °C.

Nested RT-PCR was performed to amplify the *Pcif1* mRNA fragment[86]. Two pairs of Pcif1 primers were designed: the first pair was identical to standard PCR primers, while the second pair bound to an internal region of the first PCR product (Supplementary Data 1), resulting in a shorter amplicon during the second RT-qPCR amplification. To ensure data reliability, we implemented rigorous quality control measures, including the use of reverse transcriptase-negative controls, post-collection imaging to confirm single-cell isolation, and PCR amplification of key cellular markers—such as *Rbp4* for S1L5 excitatory neurons, *Drd3* for S1L2/3 excitatory neurons, *Ntsr1* for S1L6 excitatory neurons, *Gad1* for inhibitory neurons, *NeuN* as a pan-neuronal marker, *Gfap* for astrocytes, and *Gapdh* as a loading control. These steps were followed by gel electrophoresis to exclude potential contamination from adjacent cortical layers.

Laser capture microdissection

Fluorescently labeled neurons in the S1HL region were isolated using laser capture microdissection[87]. The mouse brain was removed and then rapidly frozen in OCT compound using dry liquid nitrogen. The S1HL slices were sectioned (15 mm) using a cryostat (Leica Microsystems Wetzlar, Germany) and placed on an RNase-free glass slide. A single S1HL neuron was obtained using a laser microdissection system (LMD7000; Leica Microsystems). 20 neurons were pooled into one same sample for qPCR analysis.

Analysis of SERBP1-PCIF1 protein interaction

Protein sequences were submitted to AlphaFold Server (https://alphafoldserver.com) with default parameters[88]. The predicted models were validated by assessing the pLDDT (predicted lDDT-Cα) confidence scores, retaining the model with the highest pLDDT score for further analysis. The predicted structures were refined using the "Repair PDB" function in the FoldX (http://foldxsuite.crg.eu/) plugin within YASARA (YASARA Biosciences: www.yasara.org). PyMOL (http://www.pymol.org/pymol) was employed for structural visualization and measurement of hydrogen bond distances of amino acids that may be involved in binding. To evaluate residue-specific binding contributions, alanine scanning mutagenesis was systematically performed using FoldX's position scan protocol[89]. Key candidate residues were substituted with alanine to calculate binding free energy changes (ΔΔG) between SERBP1 and PCIF1. Hydrogen bonds with donor-acceptor distances <3.5 Å were considered stable, ensuring optimal orbital overlap and electrostatic interactions[90]. Residues with ΔΔG > 2 kcal/mol upon alanine substitution were defined as energetically critical for the interaction[89].

m^6Am-Exo-seq

11 μg of mRNAs were mixed with NEBNext® Magnesium RNA Fragmentation buffer (E6150, NEB) on ice and incubated at 94 °C for 2 min to generate fragments of 200–300 bp, and purified using the RNA Cleanup & Concentration Kit (T2030, NEB) and eluted in 20 μL elution buffer. The purified mRNAs were treated with 20U T4 PNK (T0201, NEB) in T4 ligase buffer at 37 °C to phosphorylate uncapped and fragmented transcripts. Subsequently, XRN-1 (M0338, NEB), a 5′-phosphate-dependent exonuclease, was added to specifically digest the phosphorylated (uncapped and sheared) transcripts. Thus, 5′-capped transcript-enriched RNAs were left and purified using the RNA Cleanup & Concentration Kit. The mRNA decapping Enzyme (M0608, NEB) was added to remove m^7G caps at 37 °C for 30 min, and then repurified with the RNA Cleanup & Concentration Kit and eluted

in 20 µL buffer. As a result, approximately 1 µg of decapped 5′ RNA fragments were obtained for subsequent analysis. 1 µL (10%) of processed RNAs were used as input control, while the remainders were diluted with reaction buffer (1× DEPC-PBS + 0.5% Tween-20) to a final volume of 400 µL. Protein A/G Magnetic Beads (HY-K0202, MCE) were prepared by washing four times with 1 mL binding/wash buffer, then resuspended in 400 µL reaction buffer containing 4 µg anti-m^{6}A antibody (A22411, ABclonal). After 2 h rotational incubation at 4 °C, the bead-antibody complexes were washed twice with 1 mL ice-cold binding/wash buffer. Then, the complexes were combined with RNA in 400 µL reaction buffer and incubated overnight at 4 °C with rotation. Bead-bound mRNAs were subsequently eluted using phenol-chloroform extraction and purified by RNA Cleanup & Concentration Kit.

Sequencing library preparation were conducted by Majorbio Co., Ltd. (Shanghai, China) using the SMART-Seq_V4 protocol (Clontech; San Diego, CA). Polyadenylated mRNA was reverse-transcribed from 10 ng total RNA using Oligo(dT) primers and MMLV reverse transcriptase, and generated single-stranded cDNA with 3′-terminal CCC overhangs, and amplified to nanogram-scale cDNA quantities using PCR. Subsequent fragmentation and adapter ligation were achieved through Tn5 transposase-mediated enzymatic cleavage coupled with end repair. Final library validation included quantification via Qubit 4.0 fluorometry prior to paired-end sequencing (2 × 150 bp) on the Nova-Seq X Plus platform. Raw sequencing paired-end reads first underwent adapter trimming and quality assessment using fastp[91] with default parameters.

The m^{6}Am-Exo-seq data analyses were performed using protocols adapted from established methods[21,25,55], with modifications as described below. Briefly, paired-end sequencing reads were first processed with Trimmomatic (v0.39)[92] to remove adapters and low-quality bases. The cleaned reads were then aligned to the mouse reference genome (mm10) using HISAT2 (v2.1.0)[93]. To identify putative m6Am peaks, MACS2 (v2.1.1)[94] was used with the following parameters: an effective genome size of 2.7×10^9, the -nomodel option enabled, and a q-value cutoff of 0.05. Before peak calling, input samples were normalized to ensure equal sequencing depth. For motif analysis, consensus peaks from three biological replicates were identified through reciprocal overlap. Sequences spanning ±50 bp from peak centers were extracted from the sense strand. De novo motif discovery was then performed using MEME (v5.5.7)[95]. For metagene analysis, the GenomicRanges (v1.60.0) and Guitar (v2.24.0) packages in R were utilized, employing gene annotations derived from TxDb.Mmusculus.UCSC.mm10.knownGene.

To identify differentially expressed genes (DEGs) between two samples, the expression level of each transcript was calculated using the gene counts method, where single gene counts equals RIP-gene counts minus the corresponding input gene counts. Additionally, Gene Ontology (GO) enrichment analysis was performed to determine which DEGs were significantly enriched in specific GO terms, applying a Bonferroni-corrected P-value threshold of <0.05 compared to the whole transcriptome background. GO functional enrichment analyses were conducted using tools available at https://hiplot.cn and https://www.webgestalt.org.

SERBP1-RIP-seq

S1HL tissues were harvested from mice anesthetized with isoflurane. Tissues from four mice were pooled to create a single sample. Sample was homogenized in RIP lysis buffer (150 mM KCl, 25 mM Tris pH 7.4, 5 mM EDTA, 0.5 mM DTT, 0.5% NP4, RNAse inhibitor, protease inhibitor), and incubated on ice for 30 min. Following centrifugation, the supernatant was collected and incubated with Anti-SERBP1 antibody overnight at 4 °C with gentle agitation. Subsequently, 100 µL of pre-washed protein A/G magnetic beads (HY-K0202, MCE) were added, and the mixture was incubated at room temperature for 2 h with rotation. RNAs bound to the beads were then eluted using phenol-chloroform extraction. RNA sequencing library was prepared using the SMART-Seq_V4 Ultra Low Input RNA Kit for Sequencing from Clontech (San Diego, CA). RNA sequencing, quality control, and data analysis were performed as described for m^{6}Am-Exo-Seq.

RNC sequencing

Mouse tissue was removed rapidly and placed in 0.5 mL RB buffer (20 mM HEPES-KOH (pH 7.4), 15 mM $MgCl_2$, 200 mM KCl, 100 µg/mL cycloheximide, 2 mM dithiothreitol) with 1% Triton, 5 µl PMSF (100 mM), and 200 U RNase inhibitor for each sample. The lysate was then incubated on ice for 30 min. Then it was centrifuged (11,000 × g, 10 min at 4 °C) and discard the precipitate. Take 10% supernatant liquid as the Input control, and slowly add 90% supernatant liquid to the upper layer of 9.5 mL sucrose buffer (30% sucrose in RB buffer). Polyribosome precipitate was collected after centrifuge (127,000 × g, 5 h at 4 °C). RNA was isolated from Input and polyribosome precipitation, and then submitted to Majorbio Co., Ltd. (Majorbio, China) for transcriptome sequencing. FPKM (fragments per kilobase per million) was used to normalize gene expression levels. RNA sequencing, quality control, and data analysis were performed according to the m^{6}Am-Exo-Seq protocol described above. Translation efficiency (TE) was determined by the ratio of FPKM in polyribosome-seq to FPKM in input RNA-seq.

LC–MS/MS

We quantified m^{6}Am levels in the mRNA of S1HL (somatosensory cortex of the hind limb) using an LC–MS/MS assay[25]. Total RNA was extracted by RNAiso reagent (9108, Taraka). Extracting mRNA from 30ug total RNA by BeyoMag™ mRNA purification kit with magnetic beads (R0071L, Beyotime). The mRNA decapping Enzyme (M0608, NEB) was added to remove m7G caps, and then enzymatically hydrolyzed to nucleosides by Nucleoside Digestion Mix (M06459S, NEB), and extracted with phenol–chloroform. The upper clear aqueous layer was collected and filtered through 0.22 µm Millex-GV filters (EMD Millipore) into vials. Agilent 6410 QQQ triple-quadrupole LC mass spectrometer was used for mass spectrometry detection. Chromatographic separation was conducted on an Agilent 1290 Infinity II UHPLC platform equipped with a ZORBAX RRHD Eclipse Plus C18 analytical column (150 × 2.1 mm ID, 1.8 µm particle size) coupled to a matching guard column (5 × 3 mm ID, 1.8 µm; Agilent). The mobile phase comprised water and methanol (each containing 0.1% formic acid) delivered at 0.23 mL/min. The gradient program initiated with 5% methanol (0.5 min), followed by sequential steps: 5% → 15% methanol over 2.5 min, 15% → 95% methanol over 3 min, and column re-equilibration at 5% methanol for 4 min. For unmodified ribonucleoside analysis, samples were diluted and analyzed under isocratic conditions with 20% methanol. Mass detection employed an Agilent 6495 Triple Quadrupole mass spectrometer with positive electrospray ionization. RNA modification ratios (m^{6}Am/A, m^{6}A/A, ac^{4}C/C, m^{5}C/C, and m^{7}G/G) were quantified using Agilent MassHunter software by integrating AUC values from mass spectrometry chromatograms[25].

AAV plasmid construction and virus production

Full-length *Pcif1*, *Serbp1*, and *Maf1* cDNA was amplified from mouse cortex cDNA, and the corresponding AAV virus with *CaMK2α* promoter were constructed. Primer sequences are listed in Supplementary Data 1. All constructed plasmids were confirmed by DNA sequencing. Viruses were generated in AAV293 cells, purified using an AAVpro Purification Kit (6232, Takara), and titrated with an AAVpro Titration Kit (6666, Takara). BALB/c mice were specifically employed for the initial validation of viral constructs and pilot experiments because of their increased susceptibility to viral transduction.

Cell line culture and transfection
HEK293T(H4-1401) and HT22(M8-0201) cells were purchased from Oricell, and authenticated by STR profiling. HT22 and HEK293T cells were cultured in DMEM with 10% fetal bovine serum at 37 °C in a humidified incubator. Cells were transfected with plasmid using ExFect Transfection Reagent (T101, Vazyme) following the manufacturer's instructions.

CRISPR vector specifically targeting the m^{6}Am site in *Maf1*
Full-length Pcif1 was cloned into BamHI-digested EF1a-dCasRx-2A-EGFP using the ClonExpress II one-step cloning kit (C112, Vazyme). Lentivirus gRNAs, including gRNA-26 (targeting +26 to +64 of Maf1 mRNA) and gRNA-60 (targeting +60 to +79), along with a negative control gRNA, were constructed by ligating to pLH-sgRNA1 using the primers listed in Supplementary Data 1. Lentivirus was collected by transfecting HEK293T cells with a lentiviral expression construct and identified by DNA sequencing.

Protein mass spectrometry
We constructed a PCIF1-HA overexpression construct and fully transfected it into human HEK293T and murine HT22 cells (n = 2). The PCIF1 protein was pulled down using an HA-tag (AE105) antibody and subjected to proteomic analysis by GeneChem (Shanghai, China). LC-MS/MS was performed using a Q Exactive mass spectrometer coupled with an Easy nLC system (Thermo Fisher Scientific, MA, USA). Raw data were processed in Proteome Discoverer 2.2 (Thermo Fisher Scientific) for protein identification, followed by database searching using the embedded Mascot 2.6 engine. Protein identification was conducted against a custom database (detailed in the Chinese "Methods" section). Search parameters included: trypsin as the digestion enzyme with ≤2 missed cleavages; precursor mass tolerance of 10 ppm; fragment mass tolerance of 0.05 Da; carbamidomethylation (C) as a fixed modification; and oxidation (M) and acetylation (protein N-terminus) as variable modifications. Proteins were considered positively identified if at least one unique peptide achieved a significance threshold of FDR ≤ 0.01.

PCIF1-MTase protein expression in vitro and purification
The coding sequence of mouse PCIF1-MTase domain was cloned as an in-frame fusion to the His tagged vector PLou3. The PLou3-MTase expression vector was transformed into BL21(DE3) competent cells for protein expression. Induction of protein expression was carried out with 0.5 mM IPTG at 18 °C overnight. Bacteria were harvested at 1252 × *g*, 4 °C and the cell pellet was resuspended in protein purification lysis buffer (50 mM Tris-HCl pH 7.5, 0.25 M NaCl, 0.1% Triton-X, 1 mM PMSF, 1 mM DTT, and protease inhibitors) and lysed using an ultrasonic cell disruptor under low-temperature conditions with the following parameters: 30% amplitude (600 W), 3 s pulse duration, 5 s interval, and 2 min operation cycles followed by 2 min cooling periods until the solution became clear. The lysate was collected and centrifuged at 11,000 × *g* for 15 min at 4 °C to separate the supernatant from the pellet. For protein purification, the pre-packed Ni-NTA affinity column was equilibrated with 5 column volumes of lysis buffer. The clarified supernatant was then loaded onto the equilibrated column and allowed to incubate for at least 2 min to ensure sufficient interaction between the target protein and the resin. The flow-through was collected, and the column was washed with 10–15 column volumes of wash buffer to remove non-specifically bound proteins. Finally, the target protein was eluted using 5–10 column volumes of elution buffer with fraction collection. The purification efficiency was assessed by SDS-PAGE analysis.

In vitro methyltransferase assays
The 5′UTR mRNA was isolated following the m^{6}Am-Exo-Seq protocol. In vitro methylation reactions were performed in a 50 µL system containing 50 nM MTase, SERBP1 protein (purchased from AtaGenix, China), and 4 µM 5′UTR mRNA in methylation buffer (50 mM Tris-HCl, pH 8.0, 1 mM EDTA, 1 mM DTT, 5% glycerol) supplemented with 160 µM S-adenosylmethionine (B9003, NEB). The reaction mixture was incubated at 37 °C for 10 min, followed by heat inactivation at 65 °C for 20 min. RNA purification was carried out using the RNA Cleanup & Concentration Kit (T2030, NEB) according to the manufacturer's instructions. The purified RNA samples were filtered through a 0.22 µm Millex syringe filter (Millipore) and subsequently subjected to LC-MS analysis for m^{6}Am quantification.

Western blotting
After anesthetizing mice with isoflurane and perfusing them with physiological saline, S1HL tissue was taken from the mice. The collected tissue was washed twice with precooled PBS and lysed in RIPA buffer (P0013B, Beyotime). Following centrifugation at 11,000 × *g* for 15 min at 4 °C, the supernatant was collected and its concentration quantified using a BCA kit (P0012S, Beyotime). Following a 2 h block with 5% skimmed milk, the membranes were incubated overnight at 4 °C with primary antibodies (PCIF1, A21596, ABclonal; SERBP1, 10729-1-AP, Proteintech; MAF1, A15531, ABclonal). Following three 5 min rinses, the membranes were incubated with the appropriate secondary antibody (Beyotime) for 2 h at room temperature. The membranes were rinsed three times for 5 min each with TBS-Tween. Detection was conducted using ECL reagent (P0018FS, Beyotime) and a UVITEC System (Q9 Alliance, UVITEC). Protein bands were quantified using ImageJ software and normalized to H3 or β-Actin bands.

Co-immunoprecipitation (Co-IP)
Co-IP assay was conducted using an immunoprecipitation kit with protein A + G magnetic beads (P2179S, Beyotime) following the manufacturer's protocol. The antibodies PCIF1 and SERBP1 were utilized in co-IP assays, with murine IgG and rabbit IgG serving as negative controls.

Immunohistochemistry
Animals were anesthetized with isoflurane and perfused with 4% paraformaldehyde. Then, the brains were taken out and postfixed for 6 h at 4 °C. Brains were dehydrated using 30% sucrose and sectioned at 30 µm with a freezing sledge microtome. The sections were washed thrice for 10 min in PBS, then blocked with 10% donkey serum and 0.4% Triton X-100 in PBS for 2 h. After three PBS rinses, the sections were incubated with the following primary antibodies at 4 °C for one or two nights: PCIF1 (1:500, A21596, ABclonal), NeuN (1:500, ab104224, Abcam), Iba1 (1:500, ab3554, Abcam), S-100β (1:500, S2532, Sigma), SERBP1 (1:500, 10729-1-AP, Proteintech), and MAF1 (1:500, A15531, ABclonal). After washing three times (10 min each) with PBS, the sections were incubated for 2 h at room temperature with the fluorescein-conjugated secondary antibody. Finally, the sections were stained with DAPI and examined using Olympus FV1000 laser confocal microscope.

In vivo calcium imaging
Localized calcium signals were recorded by fiber photometry of GCaMP6s fluorescence. Mice were injected with AAV-DIO-GCaMP6s (PT-0071, BrainVTA) and implanted with optical fibers prior to behavioral tests and fiber photometry recordings in S1HL. The fiber photometry system (Inper) has been described previously. The laser power at the tip of the optical fiber was adjusted to 20–40 µW. The photomultiplier tube current output was amplified and converted into a voltage signal by an amplifier, then digitized at 50 Hz and recorded by Inper-Studio software (Inper). Heatmaps and averaged Ca^{2+} traces were plotted with custom-written functions in InperDataProcess and GraphPad Prism. The raw photometry signal (X) was converted to Z-Scores: Z-Score = (X − mean)/standard deviation. The sample mean and standard deviation refer to values calculated from the 3 s before

the stimulus. This approach was applied to the analysis of data collected before and after von Frey stimulation. We checked and verified that the photometry signals were free of movement artifacts: the eGFP signal originating from control AAV2/9-DIO-eGFP (PT-0086, BrainVTA) expression in $S1HL^{Glu}$ neurons did not change during epochs of pain behavior.

Brain slice electrophysiology

Mice were anesthetized with 2% isoflurane and intracardially perfused with 20 mL oxygenated ice-cold sACSF containing 85 mM NaCl, 24 mM $NaHCO_3$, 1.25 mM NaH_2PO_4, 4.0 mM $MgCl_2$, 2.5 mM KCl, 0.5 mM $CaCl_2$, 75 mM sucrose, and 25 mM glucose. The brain was then sliced into 300 μm coronl sections containing S1HL using a vibrating microtome (VT1200s, Leica). Brain slices were incubated in ACSF (125 mM NaCl, 26 mM $NaHCO_3$, 1.2 mM NaH_2PO_4, 1.2 mM $MgCl_2$, 2.5 mM KCl, 2.4 mM $CaCl_2$, 11 mM glucose) for a minimum of 1 h at 32 °C. The brain slices were transferred to recording chamber and were perfused with ACSF at 3 ± 0.5 mL/min.

For electrophysiological recordings, an infrared (IR) differential interference contrast (DIC) microscope (BX51WI, Olympus) equipped with for fluorescence detection was used to visualize neurons in S1 slices. Whole-cell patch-clamp recordings were performed using a MultiClamp 700B amplifier, a Digidata 1440 A analog-to-digital converter, and pClamp 10.7 software (Axon Instruments/Molecular Devices). Pipettes (4–10 megaohms) made of borosilicate glass (VitalSense Scientific Instruments) were pulled using a horizontal puller (P1000, Sutter Instruments). Current-evoked action potential firing was recorded in current-clamp mode with internal solution containing 135mM K-gluconate, 5 mM KCl, 0.2 mM EGTA, 0.5 mM $CaCl_2$, 10 mM HEPES, 2 Mg-ATP, 0.1 mM GTP. (osmolarity: 300 mOsm/kg, pH: 7.2). The above records were sampled at 10 kHz and filtered at 2 kHz. All experiments were conducted at room temperature (22–24 °C).

RNA immunoprecipitation

S1HL tissue was removed from mice and homogenized in RIP lysis buffer with a glass homogenizer. After centrifugation, the supernatant was sonicated and divided into three aliquots: Input, IgG, and IP. Anti-m^6A antibody or IgG was added, respectively to the IP and IgG samples, and the mixture was incubated overnight at 4 °C. Then, magnetic beads were added and the mixture was incubated for another 2 h. The RNA adsorbed by the beads was eluted and extracted by TRIzol. Four pairs of primers were designed: the first two pairs were located in the 5′ UTR region, covering the m^6Am site (1st [F1R1]: +1 – +80; 2nd [F1R2]: +1 – +94, with the first nucleotide of mRNA designated as +1); the last two pairs were in the CDS (3rd [F3R3]: +516 – +669) and the 3′UTR (4th [F4R4]: +955 - +1109) regions. RT-qPCR was used to detect the m^6Am levels in different regions of *Maf1* mRNA. The PCR primers are shown in Supplementary Data 1.

Mammalian two-hybrid assay

To identify the domains of SERBP1 that interact with PCIF1, we carried out an in vitro mammalian two-hybridization experiment using a three-plasmid system: the pACT plasmid (encoding the herpes simplex virus VP16 activation domain upstream of an MCR and expressing the Renilla reniformis luciferase), the pBIND plasmid (encoding the yeast GAL4 DNA binding domain upstream of a multiple cloning region, MCR), and the reporter plasmid pG5luc (encoding firefly luciferase) were purchased from Promega (CheckMate Mammalian Two-Hybrid System). Four domains of *Pcif1*— the N terminal WW domain, helical, methyltransferase (MTase), and C-terminal domains, respectively inserted into the pACT vector to form five pACT-Pcif1-X construer (X represents the individual domain) through amplifing from mouse cDNA using primers (Supplementary Data 1). The full-length *Serbp1* CDS was cloned into the pBIND vector (pBIND-Serbp1) to generate a Gal4-Serbp1 chimeric fusion protein (Fig. 4c). The determination of the interaction of SERBP1 with the specified PCIF1 domain was measured through the pG5luc luciferase level after cotransfection of the vectors in HEK293T cells. All constructs were verified by PCR and DNA sequencing. Detection of the reporter was carried out according to the manufacturer's instructions.

Optogenetic manipulation

We used CIBN and CRY2[96] optogenetic approach to evaluate the effect of the interaction of SERBP1 and PCIF1 on deposition of m^6Am level in RNA. Full-length *Pcif1* and *Serbp1* were inserted into Lenti-EF1α-Pcif1-Cibn and Lenti-EF1α-Serbp1-Cry2. For the in vitro experiment, both constructed plasmids were transfected into HT22 cells and 12 h treatment with 470 nm light (3-W energy, 4 h full light) was used to activate binding of CIBN to CRY2. Total RNA was extracted at 40 h after light treatment, and the m^6Am level was analyzed via LC–MS/MS. For the in vivo experiment, Lenti-EF1α-Pcif1-Cibn and Lenti-EF1α-Serbp1-Cry2 were co-microinjected into S1HL of naïve mice, followed by implantation of optical fibers. 7 days after injection, mice were subjected to 465 nm light stimulation with the following laser parameters: 5 mW energy, 5 Hz pulse frequency, 100 ms pulse width, 5 s stimulation duration, 1 s interstimulus interval, 30 min total duration. Paw withdrawal frequencies to a mechanical stimulus (von Frey hairs) were recorded. Control group mice were injected with an empty virus.

Statistics and reproducibility

Statistical analysis was performed in GraphPad 8.0 software[85]. All experiments are repeated at least three times. Sample sizes were determined empirically according to literature in the field and our previous experience[38]. Animals were randomly assigned to experimental groups in all experiments. All behavioral experiments employed double-blind testing. To rule out the influence of locomotor impairments on behavior tests, we evaluated locomotor function by measuring the distance traveled in the open field test. Data are expressed as mean ± SEM. The study assumed normal data distributions without formal testing. Statistical analysis was performed using one-way or two-way ANOVAs, as well as paired or unpaired Student's t tests. p value below 0.05 was deemed statistically significant.

Reporting summary

Further information on research design is available in the Nature Portfolio Reporting Summary linked to this article.

Data availability

The mass spectrometry proteomics data have been deposited to the ProteomeXchange Consortium (https://proteomecentral.proteomexchange.org) via the iProX partner repository[97,98] with the dataset identifier PXD065634. The RNA-seq raw data generated in this study have been deposited in the National Center for Biotechnology Information SRA database under the reference PRJNA1282680, PRJNA1282880, PRJNA1282644. Source data are provided as a Source Data file. Source data are provided with this paper.

References

1. van Hecke, O., Austin, S. K., Khan, R. A., Smith, B. H. & Torrance, N. Neuropathic pain in the general population: a systematic review of epidemiological studies. *Pain* **155**, 654–662 (2014).
2. Attal, N., Bouhassira, D. & Colvin, L. Advances and challenges in neuropathic pain: a narrative review and future directions. *Br. J. Anaesth.* **131**, 79–92 (2023).
3. Mills, S. E. E., Nicolson, K. P. & Smith, B. H. Chronic pain: a review of its epidemiology and associated factors in population-based studies. *Brit J. Anaesth.* **123**, e273–e283 (2019).
4. Li, X. Y. et al. Alleviating neuropathic pain hypersensitivity by inhibiting PKMzeta in the anterior cingulate cortex. *Science* **330**, 1400–1404 (2010).

5. Jin, Y. et al. A somatosensory cortex input to the caudal dorsolateral striatum controls comorbid anxiety in persistent pain. *Pain* **161**, 416–428 (2020).
6. Damasio, A. R. et al. Subcortical and cortical brain activity during the feeling of self-generated emotions. *Nat. Neurosci.* **3**, 1049–1056 (2000).
7. Talbot, J. D. et al. Multiple representations of pain in human cerebral cortex. *Science* **251**, 1355–1358 (1991).
8. De Ridder, D., De Mulder, G., Menovsky, T., Sunaert, S. & Kovacs, S. Electrical stimulation of auditory and somatosensory cortices for treatment of tinnitus and pain. *Prog. Brain Res.* **166**, 377–388 (2007).
9. Fitzcharles, M. A. et al. Nociplastic pain: towards an understanding of prevalent pain conditions. *Lancet* **397**, 2098–2110 (2021).
10. Liu, Y. et al. Touch and tactile neuropathic pain sensitivity are set by corticospinal projections. *Nature* **561**, 547–550 (2018).
11. Ishikawa, T. et al. Pain-related neuronal ensembles in the primary somatosensory cortex contribute to hyperalgesia and anxiety. *iScience* **26**, 106332 (2023).
12. Pancholi, R., Ryan, L. & Peron, S. Learning in a sensory cortical microstimulation task is associated with elevated representational stability. *Nat. Commun.* **14**, 3860 (2023).
13. Ziegler, K. et al. Primary somatosensory cortex bidirectionally modulates sensory gain and nociceptive behavior in a layer-specific manner. *Nat. Commun.* **14**, 2999 (2023).
14. Barbieri, I. & Kouzarides, T. Role of RNA modifications in cancer. *Nat. Rev. Cancer* **20**, 303–322 (2020).
15. Wei, C., Gershowitz, A. & Moss, B. N6, O2′-dimethyladenosine a novel methylated ribonucleoside next to the 5′ terminal of animal cell and virus mRNAs. *Nature* **257**, 251–253 (1975).
16. Grozhik, A. V. & Jaffrey, S. R. Distinguishing RNA modifications from noise in epitranscriptome maps. *Nat. Chem. Biol.* **14**, 215–225 (2018).
17. Keith, J. M., Ensinger, M. J. & Moss, B. HeLa cell RNA (2′-O-methyladenosine-N6-)-methyltransferase specific for the capped 5′-end of messenger RNA. *J. Biol. Chem.* **253**, 5033–5039 (1978).
18. Liu, Z., Lan, P., Liu, T., Liu, X. & Liu, T. m6Aminer: predicting the m6Am sites on mRNA by fusing multiple sequence-derived features into a CatBoost-Based Classifier. *Int. J. Mol. Sci.* **24**, 7878 (2023).
19. Akichika, S. et al. Cap-specific terminal N 6-methylation of RNA by an RNA polymerase II-associated methyltransferase. *Science* **363**, eaav0080 (2019).
20. Boulias, K. et al. Identification of the m6Am methyltransferase PCIF1 reveals the location and functions of m6Am in the transcriptome. *Mol. Cell* **75**, 631–643.e638 (2019).
21. Sendinc, E. et al. PCIF1 catalyzes m6Am mRNA methylation to regulate gene expression. *Mol. Cell* **75**, 620–630.e629 (2019).
22. Sun, H., Zhang, M., Li, K., Bai, D. & Yi, C. Cap-specific, terminal N6-methylation by a mammalian m6Am methyltransferase. *Cell Res.* **29**, 80–82 (2019).
23. Li, K. et al. The CTBP2-PCIF1 complex regulates m6Am modification of mRNA in head and neck squamous cell carcinoma. *J. Clin. Investig.* **133**, e170173 (2023).
24. Relier, S. et al. FTO-mediated cytoplasmic m6Am demethylation adjusts stem-like properties in colorectal cancer cell. *Nat. Commun.* **12**, 1716 (2021).
25. Zhuo, W. et al. m6Am methyltransferase PCIF1 is essential for aggressiveness of gastric cancer cells by inhibiting TM9SF1 mRNA translation. *Cell Discov.* **8**, 48 (2022).
26. Wang, L. et al. Role of PCIF1-mediated 5′-cap N6-methyladeonsine mRNA methylation in colorectal cancer and anti-PD-1 immunotherapy. *EMBO J.* **42**, e111673 (2023).
27. Zhang, Q. et al. HIV reprograms host m6Am RNA methylome by viral Vpr protein-mediated degradation of PCIF1. *Nat. Commun.* **12**, 5543 (2021).
28. Cong, S. et al. Integrative proteomic and lipidomic analysis of Kaili Sour Soup-mediated attenuation of high-fat diet-induced non-alcoholic fatty liver disease in a rat model. *Nutr. Metab.***18**, 26 (2021).
29. Heaton, J. H., Dlakic, W. M., Dlakic, M. & Gelehrter, T. D. Identification and cDNA cloning of a novel RNA-binding protein that interacts with the cyclic nucleotide-responsive sequence in the Type-1 plasminogen activator inhibitor mRNA. *J. Biol. Chem.* **276**, 3341–3347 (2001).
30. Go, C. D. et al. A proximity-dependent biotinylation map of a human cell. *Nature* **595**, 120–124 (2021).
31. Shilenok, I. et al. SERPINE1 mRNA binding protein 1 is associated with ischemic stroke risk: a comprehensive molecular-genetic and bioinformatics analysis of SERBP1 SNPs. *Int. J. Mol. Sci.* **24**, 8716 (2023).
32. Youn, J. Y. et al. High-density proximity mapping reveals the subcellular organization of mRNA-associated granules and bodies. *Mol. Cell* **69**, 517–532.e511 (2018).
33. Ma, L. et al. ZNF382 controls mouse neuropathic pain via silencer-based epigenetic inhibition of Cxcl13 in DRG neurons. *J. Exp. Med.* **218**, e20210920 (2021).
34. Wang, D. et al. Lateral septum-lateral hypothalamus circuit dysfunction in comorbid pain and anxiety. *Mol. Psychiatr.* **28**, 1090–1100 (2023).
35. Cichon, J., Blanck, T. J. J., Gan, W. B. & Yang, G. Activation of cortical somatostatin interneurons prevents the development of neuropathic pain. *Nat. Neurosci.* **20**, 1122–1132 (2017).
36. Kim, W., Kim, S. K. & Nabekura, J. Functional and structural plasticity in the primary somatosensory cortex associated with chronic pain. *J. Neurochem.* **141**, 499–506 (2017).
37. Okada, T. et al. Pain induces stable, active microcircuits in the somatosensory cortex that provide a therapeutic target. *Sci. Adv.* **7**, eabd8261 (2021).
38. Zhang, M. et al. The Cytidine N-Acetyltransferase NAT10 Participates in Peripheral Nerve Injury-Induced Neuropathic Pain by Stabilizing SYT9 Expression in Primary Sensory Neurons. *J. Neurosci.* **43**, 3009–3027 (2023).
39. Gradinaru, V., Mogri, M., Thompson, K. R., Henderson, J. M. & Deisseroth, K. Optical deconstruction of Parkinsonian neural circuitry. *Science* **324**, 354–359 (2009).
40. Cassidy, R. M. et al. A lateral hypothalamus to basal forebrain neurocircuit promotes feeding by suppressing responses to anxiogenic environmental cues. *Sci. Adv.* **5**, eaav1640 (2019).
41. Bordi, M. et al. Autophagy flux in CA1 neurons of Alzheimer hippocampus: Increased induction overburdens failing lysosomes to propel neuritic dystrophy. *Autophagy* **12**, 2467–2483 (2016).
42. Onodera, K. & Kato, H. K. Translaminar recurrence from layer 5 suppresses superficial cortical layers. *Nat. Commun.* **13**, 2585 (2022).
43. Ping, X. L. et al. Mammalian WTAP is a regulatory subunit of the RNA N6-methyladenosine methyltransferase. *Cell Res* **24**, 177–189 (2014).
44. Jumper, J. et al. Highly accurate protein structure prediction with AlphaFold. *Nature* **596**, 583–589 (2021).
45. Nantasenamat, C., Prachayasittikul, V. & Bulow, L. Molecular modeling of the human hemoglobin-haptoglobin complex sheds light on the protective mechanisms of haptoglobin. *PLoS ONE* **8**, e62996 (2013).
46. Kennedy, M. J. et al. Rapid blue-light-mediated induction of protein interactions in living cells. *Nat. Methods* **7**, 973–975 (2010).
47. Linder, B. et al. Single-nucleotide-resolution mapping of m6A and m6Am throughout the transcriptome. *Nat. Methods* **12**, 767–772 (2015).
48. Lorsch, Z. S. et al. Stress resilience is promoted by a Zfp189-driven transcriptional network in prefrontal cortex. *Nat. Neurosci.* **22**, 1413–1423 (2019).

49. Hofacker, D. et al. Engineering of effector domains for targeted DNA methylation with reduced off-target effects. *Int. J. Mol. Sci.* **21**, 502 (2020).
50. Lai, C. et al. Maf1 suppression of ATF5-dependent mitochondrial unfolded protein response contributes to rapamycin-induced radio-sensitivity in lung cancer cell line A549. *Aging* **13**, 7300–7313 (2021).
51. Palian, B. M. et al. Maf1 is a novel target of PTEN and PI3K signaling that negatively regulates oncogenesis and lipid metabolism. *PLoS Genet* **10**, e1004789 (2014).
52. Han, Y. et al. Maf1 loss regulates spinogenesis and attenuates cognitive impairment in Alzheimer's disease. *Brain 16, awae015*, (2024).
53. Smith, K. R. et al. Identification and characterisation of a Maf1/Macoco protein complex that interacts with GABAA receptors in neurons. *Mol. Cell. Neurosci.* **44**, 330–341 (2010).
54. Sun, H., Li, K., Liu, C. & Yi, C. Regulation and functions of non-m6A mRNA modifications. *Nat. Rev. Mol. Cell Bio* **24**, 714–731 (2023).
55. Wang, L. et al. PCIF1-mediated deposition of 5′-cap N6,2′-O-dimethyladenosine in ACE2 and TMPRSS2 mRNA regulates susceptibility to SARS-CoV-2 infection. *Proc. Natl. Acad. Sci. USA* **120**, e2210361120 (2023).
56. Mauer, J. et al. Reversible methylation of m6Am in the 5′ cap controls mRNA stability. *Nature* **541**, 371–375 (2017).
57. Sikorski, P. J. et al. The identity and methylation status of the first transcribed nucleotide in eukaryotic mRNA 5′ cap modulates protein expression in living cells. *Nucleic Acids Res.* **48**, 1607–1626 (2020).
58. Liu, J. et al. Landscape and regulation of m6A and m6Am methylome across human and mouse tissues. *Mol. Cell* **77**, 426–440.e426 (2020).
59. Engel, M. et al. The role of m6A/m-RNA methylation in stress response regulation. *Neuron* **99**, 389–403.e389 (2018).
60. Chen, A. et al. Single-cell spatial transcriptome reveals cell-type organization in the macaque cortex. *Cell* **186**, 3726–3743.e3724 (2023).
61. Codeluppi, S. et al. Spatial organization of the somatosensory cortex revealed by osmFISH. *Nat. Methods* **15**, 932–935 (2018).
62. Li, Z. Z. et al. Extracellular matrix protein laminin β1 regulates pain sensitivity and anxiodepression-like behaviors in mice. *J. Clin. Investig.* **131**, e146323 (2021).
63. Schöller, E. et al. Interactions, localization, and phosphorylation of the m6A generating METTL3-METTL14-WTAP complex. *RNA* **24**, 499–512 (2018).
64. Shen, L. Functional interdependence of N6-methyladenosine methyltransferase complex subunits in Arabidopsis. *Plant Cell* **35**, 1901–1916 (2023).
65. Kosti, A. et al. The RNA-binding protein SERBP1 functions as a novel oncogenic factor in glioblastoma by bridging cancer metabolism and epigenetic regulation. *Genome Biol.* **21**, 195 (2020).
66. Tsuboyama, K. et al. A widespread family of heat-resistant obscure (Hero) proteins protect against protein instability and aggregation. *PLoS Biol.* **18**, e3000632 (2020).
67. Bolger, G. B. The RNA-binding protein SERBP1 interacts selectively with the signaling protein RACK1. *Cell. Signal.* **35**, 256–263 (2017).
68. Lee, Y. J., Hsieh, W. Y., Chen, L. Y. & Li, C. Protein arginine methylation of SERBP1 by protein arginine methyltransferase 1 affects cytoplasmic/nuclear distribution. *J. Cell. Biochem.* **113**, 2721–2728 (2012).
69. Lee, Y. J., Wei, H. M., Chen, L. Y. & Li, C. Localization of SERBP1 in stress granules and nucleoli. *FEBS J.* **281**, 352–364 (2014).
70. Shao, J. et al. Synthetic far-red light-mediated CRISPR-dCas9 device for inducing functional neuronal differentiation. *Proc. Natl. Acad. Sci. USA* **115**, E6722–e6730 (2018).
71. Zhou, H. et al. In vivo simultaneous transcriptional activation of multiple genes in the brain using CRISPR-dCas9-activator transgenic mice. *Nat. Neurosci.* **21**, 440–446 (2018).
72. Ma, H. et al. Multiplexed labeling of genomic loci with dCas9 and engineered sgRNAs using CRISPRainbow. *Nat. Biotechnol.* **34**, 528–530 (2016).
73. Zhou, H. M. et al. DNA N6-methyladenine methylase N6AMT1 controls neuropathic pain through epigenetically modifying Kcnj16 in dorsal horn neurons. *Pain* **165**, 75–91 (2024).
74. Chen, D. et al. Maf1 regulates axonal regeneration of retinal ganglion cells after injury. *Exp. Neurol.* **348**, 113948 (2022).
75. Chen, K., Zhu, L., Guo, L., Pan, Y. B. & Feng, D. F. Maf1 regulates dendritic morphogenesis and influences learning and memory. *Cell Death Dis.* **11**, 606 (2020).
76. Tsang, C. K. et al. Maf1 is an intrinsic suppressor against spontaneous neural repair and functional recovery after ischemic stroke. *J. Adv. Res.* **51**, 73–90 (2023).
77. Luo, X. et al. IL-23/IL-17A/TRPV1 axis produces mechanical pain via macrophage-sensory neuron crosstalk in female mice. *Neuron* **109**, 2691–2706.e2695 (2021).
78. Mogil, J. S. Qualitative sex differences in pain processing: emerging evidence of a biased literature. *Nat. Rev. Neurosci.* **21**, 353–365 (2020).
79. Decosterd, I. & Woolf, C. J. Spared nerve injury: an animal model of persistent peripheral neuropathic pain. *Pain* **87**, 149–158 (2000).
80. Bennett, G. J. & Xie, Y. K. A peripheral mononeuropathy in rat that produces disorders of pain sensation like those seen in man. *Pain* **33**, 87–107 (1988).
81. Furman, B. L. Streptozotocin-induced diabetic models in mice and rats. *Curr. Protoc.* **1**, e78 (2021).
82. Zhang, M., Du, W., Acklin, S., Jin, S. & Xia, F. SIRT2 protects peripheral neurons from cisplatin-induced injury by enhancing nucleotide excision repair. *J. Clin. Investig.* **130**, 2953–2965 (2020).
83. Pan, Z. et al. Methyltransferase-like 3 contributes to inflammatory pain by targeting TET1 in YTHDF2-dependent manner. *Pain* **162**, 1960–1976 (2021).
84. Yang, L. et al. DExH-box helicase 9 modulates hippocampal synapses and regulates neuropathic pain. *iScience* **27**, 109016 (2024).
85. Pan, Z. et al. Downregulation of a Dorsal Root Ganglion-Specifically Enriched Long Noncoding RNA is Required for Neuropathic Pain by Negatively Regulating RALY-Triggered Ehmt2 Expression. *Adv. Sci.***8**, e2004515 (2021).
86. Yin, H. et al. Optimization of peptide nucleic acid antisense oligonucleotides for local and systemic dystrophin splice correction in the mdx mouse. *Mol. Ther.* **18**, 819–827 (2010).
87. Sakai, A. et al. MicroRNA cluster miR-17-92 regulates multiple functionally related voltage-gated potassium channels in chronic neuropathic pain. *Nat. Commun.* **8**, 16079 (2017).
88. Abramson, J. et al. Accurate structure prediction of biomolecular interactions with AlphaFold 3. *Nature* **630**, 493–500 (2024).
89. Schymkowitz, J. et al. The FoldX web server: an online force field. *Nucleic Acids Res* **33**, W382–W388 (2005).
90. Jeffrey G. A., W. Saenger, definitions and concepts, *Hydrogen Bonding in Biological Structures*, 15–48 (1991)
91. Chen, S., Zhou, Y., Chen, Y. & Gu, J. fastp: an ultra-fast all-in-one FASTQ preprocessor. *Bioinformatics* **34**, i884–i890 (2018).
92. Bolger, A. M., Lohse, M. & Usadel, B. Trimmomatic: a flexible trimmer for Illumina sequence data. *Bioinformatics* **30**, 2114–2120 (2014).
93. Kim, D., Langmead, B. & Salzberg, S. L. HISAT: a fast spliced aligner with low memory requirements. *Nat. Methods* **12**, 357–360 (2015).
94. Feng, J., Liu, T., Qin, B., Zhang, Y. & Liu, X. S. Identifying ChIP-seq enrichment using MACS. *Nat. Protoc.* **7**, 1728–1740 (2012).

95. Bailey, T. L. et al. MEME SUITE: tools for motif discovery and searching. *Nucleic Acids Res.* **37**, W202–W208 (2009).
96. Valon L., A. MarÃn-LlauradÃ³, T. Wyatt, G. Charras, & X Trepat. Optogenetic control of cellular forces and mechanotransduction. *Nat. Commun.* **8**, 14396 (2017)
97. Ma, J. et al. iProX: an integrated proteome resource. *Nucleic Acids Res.* **47**, D1211–d1217 (2019).
98. Chen, T. et al. iProX in 2021: connecting proteomics data sharing with big data. *Nucleic Acids Res.* **50**, D1522–d1527 (2022).

Acknowledgements

This study was supported by grants from the National Natural Science Foundation of China (82371243 and 82171234 to Z-Q Pan, 82201391 to Q-H Wang, 32200818 to L Yang, 82171233 to H-J W), the Jiang Su-Specially Appointed Professor Project and the Natural Science Foundation of Jiangsu Education Department Key Project (22KJA320008 to Z-Q Pan), the Starting Grants of Excellent Talents of Xuzhou Medical University (L. Yang and Q. Wang), and the Postgraduate Research and Practice Innovation Program of Jiangsu Province Grant (KYC22-2929 to Y Huang). Mouse images in Figs. 2p, 3i, 5a, 8p, and 9 were generated by Figdraw.

Author contributions

Z.-Q.P. and J.-L.C. conceptualized and supervised this study. Z.-Q.P. and Y.H. wrote the manuscript, Z.-Q.P., S.-S.-C.W., and Y.-X.T. revised the manuscript. Y.H., G.M., S.X., R.W., Y.L., Y.Z.(Zeng), Y.Z.(Zhao), Q.W., L.Y., H.H., and L.H. performed experiments and analyzed data, X.Z., H.W. and W.S. analyzed data.

Competing interests

The authors declare no competing interests.

Additional information

Supplementary information The online version contains supplementary material available at https://doi.org/10.1038/s41467-025-62565-5.

Correspondence and requests for materials should be addressed to Jun-Li Cao, Yuan-Xiang Tao or Zhi-Qiang Pan.

Peer review information *Nature Communications* thanks the anonymous reviewer(s) for their contribution to the peer review of this work. A peer review file is available.

[1]Jiangsu Province Key Laboratory of Anesthesiology, School of Anesthesiology, Xuzhou Medical University, Xuzhou, Jiangsu, China. [2]Jiangsu Province Key Laboratory of Anesthesia and Analgesia Application Technology, XuzhouMedical University, Xuzhou, Jiangsu, China. [3]National Medical Products Administration (NMPA) Key Laboratory for Research and Evaluation of Narcotic and Psychotropic Drugs, School of Anesthesiology, Xuzhou Medical University, Xuzhou, Jiangsu, China. [4]Department of Pain Medicine, Affiliated Hospital of Xuzhou Medical University, Xuzhou, Jiangsu, China. [5]Department of Anaesthesiology, School of Clinical Medicine, Li Ka Shing Faculty of Medicine, The University of Hong Kong, Hong Kong, China. [6]Department of Anesthesiology, New Jersey Medical School, Rutgers. The State University of New Jersey, Novel ark, NJ, USA. [7]These authors contributed equally: Yue Huang, Gan Ma, Shan Xie. [8]These authors jointly supervised this work: Jun-Li Cao, Yuan-Xiang Tao, Zhi-Qiang Pan. ✉e-mail: caojl0310@aliyun.com; yuanxiang.tao@njms.rutgers.edu; zhiqiangp2002@aliyun.com